ARL-TR-9537 • Sep 2022

DEVCOM ARMY RESEARCH LABORATORY

Fast Solution of Initial Value Problems for Wave Propagation in Peridynamic Media

by George A Gazonas, Burak Aksoylu, and Raymond A Wildman

NOTICES

Disclaimers

The findings in this report are not to be construed as an official Department of the Army position unless so designated by other authorized documents.

Citation of manufacturer's or trade names does not constitute an official endorsement or approval of the use thereof.

Destroy this report when it is no longer needed. Do not return it to the originator.

ARL-TR-9537 ● SEP 2022

Fast Solution of Initial Value Problems for Wave Propagation in Peridynamic Media

by George A Gazonas
DEVCOM Army Research Laboratory

Burak Aksoylu
Texas A&M University-San Antonio

Raymond A Wildman
Sandia National Laboratories

REPORT DOCUMENTATION PAGE

Form Approved
OMB No. 0704-0188

1. REPORT DATE *(DD-MM-YYYY)*	2. REPORT TYPE	3. DATES COVERED (From - To)
September 2022	Technical Report	October 2017-November 2018

4. TITLE AND SUBTITLE
Fast Solution of Initial Value Problems for Wave Propagation in Peridynamic Media

5a. CONTRACT NUMBER

5b. GRANT NUMBER

5c. PROGRAM ELEMENT NUMBER

6. AUTHOR(S)
George A Gazonas, Burak Aksoylu, and Raymond A Wildman

5d. PROJECT NUMBER
AH80

5e. TASK NUMBER

5f. WORK UNIT NUMBER

7. PERFORMING ORGANIZATION NAME(S) AND ADDRESS(ES)
DEVCOM Army Research Laboratory
ATTN: FCDD-RLW-MB
Aberdeen Proving Ground, MD 21005-5066

8. PERFORMING ORGANIZATION REPORT NUMBER
ARL-TR-9537

9. SPONSORING/MONITORING AGENCY NAME(S) AND ADDRESS(ES)

10. SPONSOR/MONITOR'S ACRONYM(S)

11. SPONSOR/MONITOR'S REPORT NUMBER(S)

12. DISTRIBUTION/AVAILABILITY STATEMENT
Approved for public release; distribution is unlimited.

13. SUPPLEMENTARY NOTES
primary author's email: <george.a.gazonas.civ@army.mil>.

14. ABSTRACT
An inverse fast Fourier transform (IFFT) algorithm is developed to solve initial value problems (IVPs) for wave propagation in nonlocal peridynamic media. The IFFT solutions compare well with solutions obtained using Mathematica's NIntegrate function and verified using a spherical Bessel function series solution. A nonlinear dispersion relation is derived using Floquet theory for a periodic elastic medium of infinite extent, which we use to solve an IVP for a homogenized peridynamic medium using our IFFT algorithm; this solution compares well with a spherical Bessel function series solution. A local-nonlocal peridynamic correspondence principle is identified, which enables direct determination of nonlocal Fourier transform domain solutions to IVPs; the correspondence principle only requires identification of the nonlinear dispersion curve for the material and does not require definition of a micromodulus function, although the latter is implicitly defined via an integral equation. Results are useful for modeling and verification of dispersive wave propagation in large-scale peridynamic numerical simulations.

15. SUBJECT TERMS
inverse fast Fourier transform, initial value problem, correspondence principle, dispersion, nonlocal, Mathematica source code, Sciences of Extreme Materials

16. SECURITY CLASSIFICATION OF:			17. LIMITATION OF ABSTRACT	18. NUMBER OF PAGES	19a. NAME OF RESPONSIBLE PERSON
a. REPORT	b. ABSTRACT	c. THIS PAGE			George A Gazonas
Unclassified	Unclassified	Unclassified	UU	56	19b. TELEPHONE NUMBER (Include area code) 410-306-0863

Contents

List of Figures

List of Tables

1. Introduction

We reconsider the class of 1-D nonlocal wave equations studied by Beyer et al.,[1] whose solutions to initial value problems (IVPs) that arise in the linear theory of peridynamics are written in terms of an infinite series of spherical Bessel functions of the first kind, and constructed through determination of the $k^{th}-$convolution of the micromodulus or kernel function[2] with the initial condition (either displacement or velocity). Our solutions to this class of wave propagation problems, however, do not require direct use of the micromodulus function, but only the dispersion relation (cf., Eq. 2.7.6 of Kunin,[3] Eq. 13 of Silling et al.[4] or Eq. 6 of Weckner and Abeyaratne[5]) and existence of the Fourier transform of the initial condition. Fourier transformation of the peridynamic momentum balance equation and initial conditions[5] permits derivation of exact or numerical solution of the IVPs studied in Beyer et al.[1] Exact analytical IVP solutions to the local wave equation are thus obtained by inverse Fourier transform of the Fourier-domain, D'Alembert equation; for the nonlocal wave equation, a Fourier-domain D'Alembert-*like* equation is solved by numerical integration which employs an inverse fast Fourier transform (IFFT) algorithm.

Our numerical solutions* compare well with those of Beyer et al.[1] but suffer from the Gibbs phenomenon in those problems where the initial condition is only piecewise continuous and piecewise smooth; in such cases, we employ the discrete inverse Fourier transform and observe reduction of the Gibbs effect, and a dramatic speedup in solution time by employing Mathematica's IFFT algorithm.[7] Further reduction of the Gibbs effect is possible using a low pass filter, for example, herein we employ Lanczos sigma factors cf., pg. 78 of Lanczos,[8] which have been successfully used for numerical inversion of the Laplace transform in problems involving multiple jump discontinuities due to impact.[9]

Weckner and Abeyaratne[5] have also studied a number of IVPs in the linear theory of peridynamics with both continuous and discontinuous initial data using Green's function methods; their solutions to the IVPs are written in terms of spatial domain integrals involving a convolution of the initial condition with Green's functions derived using the Dirac-delta function. One solution makes use of Taylor series and

*The solutions to the IVPs in this report were originally presented[6] at the USACM Thematic Conference on Nonlocal Methods in Fracture held at the University of Texas, Austin, Texas, January 15-16, 2018.

binomial expansions of the trigonometric functions that appear in the integral that defines the Green's function to derive numerical solutions for the relaxation of a bar disturbed by a Gaussian pulse initial condition. In contrast, our solutions do not explicitly rely on the use of generalized functions, such as the Dirac-delta distribution (cf., Weckner and Abeyaratne[5]), to determine Green's functions, but only on a means for determining the inverse Fourier transform of Eq. 21; in a subsequent section, we will illustrate these solutions by employing numerical integration and IFFT routines available in Mathematica.[7] Emmrich and Weckner[10] have also derived numerical solutions to IVPs in the linear theory of peridynamics using numerical integration based on Gauss-Hermite quadrature. Beyond the solution of IVPs, more general fast Fourier transform methods have recently been developed for the solution of peridynamic boundary value problems involving transient diffusion[11] and brittle fracture.[12] Other higher-order spatial and spectral numerical techniques for solving the peridynamic equation of motion have also recently been developed by Coclite et al.[13]

Eringen[14] introduced a methodology to determine the spatial dependence of nonlocal elastic moduli from dispersion curves based on 1-D lattice dynamics, which compared well with experimental dispersion curves for aluminum.* Other relevant work akin to Eringen's determination of the spatial dependence of nonlocal elastic moduli from dispersion curves appears in the work of Weckner and Silling[16] who derive a micromodulus function from a finite set of frequency-dependent phase velocities (cf., Eq. 20 of Weckner and Silling[16]). In more recent work, Silling[17] employs a direct numerical solution (DNS) methodology that uses 1-D impact simulations on periodic elastic layers to derive values for the peridynamic horizon size and micromodulus function that are incorporated into a homogenized peridynamic model. The homogenized peridynamic model results are verified by the DNS simulations.

Finally, we show how a nonlinear dispersion relation that is derived using Floquet theory for a periodic elastic medium of infinite extent can be used to solve IVPs for homogenized peridynamic media using the IFFT methods we have developed, and

*Eringen's[14] nonlinear dispersion model for aluminum consisted of a linear chain of equally spaced, identical particles; our extension to employ Floquet theory for periodic elastic media to model the dispersion in peridynamic media follows quite naturally. The methodology described herein is not limited to a unit cell comprised of only two elastic materials but can be extended to unit cells containing any number of sublayers of arbitrary length and material properties using the recursive dispersion relations derived by Velo et al.[15]

that these solutions compare well with the series solution method of Beyer et al.[1] where it is first necessary to determine the $k^{th}-$convolution of the micromodulus function with the initial condition.

The remainder of the report is outlined as follows: Section 2 develops the governing equation of motion, dispersion relation and micromodulus function for a microelastic material. Fourier and inverse Fourier transformation relations are defined and applied to the governing equations in Section 3. A local-nonlocal correspondence principle is identified (without proof) in Section 3.1.1. A set of four IVPs with both continuous and discontinuous initial values are outlined in Section 4. Error estimates using Mathematica's "NIntegrate" function and the IFFT method appear in Section 5; comparison of these numerical solutions with exact analytical solutions and associated error estimates also appear in Section 5 and are discussed in more detail in Section 6. In Section 7 we derive a nonlinear dispersion relation for a periodically layered medium of infinite extent and use this in the solution of a homogenized peridynamic IVP with an initial displacement in the form of a Gaussian pulse. This solution compares very well with the solution using the series solution method of Beyer et al.[1] Conclusions follow in Section 8.

2. Governing Equations in the Time Domain

We consider solution of 1-D IVPs for the so-called microelastic material with the governing equation of linear momentum (cf., Eq. 11 of Silling et al.[4]) given by,

$$\begin{aligned} \rho\, \ddot{u}(x,t) &= \int_{-\infty}^{\infty} C(x'-x)\Big(u(x',t)-u(x,t)\Big)dx' \;+\; b(x,t)\,, \\ &\text{for } -\infty < x < \infty, \quad t > 0\,. \end{aligned} \tag{1}$$

The corresponding governing equation of linear momentum for a local elastic medium is given by,

$$\begin{aligned} \rho\, \ddot{u_l}(x,t) &= E\,\frac{\partial^2 u_l}{\partial x^2} \;+\; b(x,t)\,, \\ &\text{for } -\infty < x < \infty, \quad t > 0\,, \end{aligned} \tag{2}$$

where E is Young's modulus, and the displacements u and u_l correspond to the nonlocal and local problems, respectively. In this report, we will only consider problems involving initial conditions in displacement u, and zero initial particle velocity

$\dot{u} = v = 0$

$$u(x,0) = f(x), \quad \dot{u}(x,0) = 0, \quad x \in \mathbb{R}\,. \tag{3}$$

A superposed dot is used to denote the ordinary derivative of a function of time only, and we will also use a superposed dot to denote the partial derivative of a field variable with respect to time, for example,

$$v(x,t) = \frac{\partial u}{\partial t} = \dot{u}(x,t)\,. \tag{4}$$

With these conventions, Eq. 1 describes the dynamic 1-D motion of a microelastic medium where ρ is the density, $\ddot{u}$ is the particle acceleration, and $b(x,t)$ is the body force. $C(x'-x)$ denotes the real and even *micromodulus* function, such that, $C(\xi) = C(-\xi)$, $\xi \in \mathbb{R}$; as pointed out in Weckner and Abeyaratne[5] $C(\xi)$ might also have compact support so that the condition that ensures that the integral Eq. 1 converges, such that, $C(\xi) \to 0$ as $\xi \to \pm\infty$ is automatically satisfied. On substituting the expression for progressive 1-D plane-waves, such that, $u(x,t) = exp(i(kx - \omega t))$ (with wavenumber k in rad/m, angular frequency ω in rad/s, $i = \sqrt{-1}$) and $\xi = x' - x$ into Eq. 1 and using the evenness property of $C(\xi)$, results in (cf., Eq. 2.7.17 of Kunin,[3] Eq. 14 of Silling et al.[4] or Eq. 6 of Weckner and Abeyaratne[5]) the integral form of the dispersion relation in terms of the micromodulus function

$$\omega(k) \;=\; \sqrt{\rho^{-1}\int_{-\infty}^{\infty} C(\xi)\Big(1-\cos(k\,\xi)\Big)d\xi}\,. \tag{5}$$

Beyer et al.[1] study IVPs for which the micromodulus function is a normal distribution (Gaussian) with amplitude proportional to a, standard deviation σ, and with zero mean,

$$C(\xi) = \frac{a}{\sqrt{2\,\pi}\,\sigma} e^{-\frac{\xi^2}{2\,\sigma^2}}\,. \tag{6}$$

On substituting Eq. 6 into Eq. 5, and integrating, yields the nonlinear dispersion relation,

$$\omega(k) \;=\; \sqrt{\frac{a}{\rho}}\,\sqrt{1 \;-\; e^{-\frac{k^2\,\sigma^2}{2}}}\,. \tag{7}$$

Beyer et al.[1] (cf., Fig. 1 caption), further set $a = \rho = \sigma = 1$, and Eq. 7 simplifies to,

$$\omega(k) \;=\; \sqrt{1 \;-\; e^{-\frac{k^2}{2}}}\,. \tag{8}$$

A length scale parameter common to nonlocal media does not explicitly appear in Eqs. 6 or 7 but if the standard deviation in Eq. 6 is associated with Kunin's[3] or Weckner and Abeyaratne's[5] "material" length scale parameter l, then on substituting $\sigma = \frac{\sqrt{2}}{2} l$ and $a = \frac{4\,E}{l^2} = \frac{4\,\rho\,c^2}{l^2}$ into Eq. 6, results in,

$$C(\xi) = \frac{4\,E}{l^3\,\sqrt{\pi}} e^{-\frac{\xi^2}{l^2}} = \frac{4\,\rho\,c^2}{l^3\,\sqrt{\pi}} e^{-\frac{\xi^2}{l^2}}\,, \tag{9}$$

which recovers the micromodulus function given by Eq. 15_2 of Weckner and Abeyaratne[5]; here, E is Young's modulus and c is the wave speed. On substituting Eq. 9 into Eq. 5 and integrating, results in the dimensionally correct nonlinear dispersion relation (cf., Eq. 16_2 of[5]),

$$\omega(k) = \frac{2\,c}{l}\sqrt{1 - e^{-\frac{k^2\,l^2}{4}}}\,, \tag{10}$$

which, as before, can be directly obtained by setting $a = \frac{4\,\rho\,c^2}{l^2}$ and $\sigma = \frac{\sqrt{2}}{2} l$ in Eq. 7. In linear elastic media, the frequency ω is a linear function of the wavenumber k, such that, $\omega(k) = \omega = c\,k$ and therefore the phase velocity $c = \omega/k$ and group velocity $c_g = d\omega/dk$ are identical, which result in Fourier modes that travel at the same speed and are independent of frequency in the medium. As will be shown in a subsequent section, a nonlocal peridynamic medium with a Gaussian micromodulus function results in Fourier modes that change shape and travel at different speeds that exhibit normal dispersion such that, $c_g < c$; anomalous dispersion occurs when $c_g > c$.

Finally, on expanding the square root function in Eq. 10 in a power series results in,

$$\sqrt{1 - e^{-\frac{k^2\,l^2}{4}}} = \frac{k\,l}{2}\left(1 - \frac{k^2\,l^2}{16} + \frac{5\,k^4\,l^4}{1536} - \frac{k^6\,l^6}{8192} + O\left(k^8\right)\right). \tag{11}$$

On substituting Eq. 11 into Eq. 10 results in,

$$\omega(k) = c\,k\left(1 - \frac{k^2\,l^2}{16} + \frac{5\,k^4\,l^4}{1536} - \frac{k^6\,l^6}{8192} + O\left(k^8\right)\right). \tag{12}$$

The classical local dispersion relation $\omega(k) = c\,k$ is recovered as the product $k\,l \to 0$ in Eq. 12; this behavior is illustrated graphically in Fig. 2 of Weckner and Abeyaratne.[5]

3. Fourier Transformations

In this work, we employ the exponential Fourier transform denoted by $\widehat{u}$ or by $\mathcal{F}\{u\}$, for functions $u \in L^1(\mathbb{R}) \cap L^2(\mathbb{R})$, that are absolutely and square integrable functions u^*

$$\widehat{u}(k,t) = \mathcal{F}\{u(x,t) : x \to k\} \equiv \int_{-\infty}^{\infty} u(x,t)\, e^{-i\,k\,x}\, dx\,, \tag{13}$$

where $k \in \mathbb{R}$ is the Fourier transform parameter of spatial variable x, and the exponential inverse Fourier transform:

$$u(x,t) = \mathcal{F}^{-1}\{\widehat{u}(k,t) : k \to x\} \equiv \frac{1}{2\pi} \int_{-\infty}^{\infty} \widehat{u}(k,t)\, e^{i\,k\,x}\, dk\,. \tag{14}$$

On substituting Eq. 13 into Eq. 14 we arrive at the Fourier integral theorem:

$$u(x,t) = \frac{1}{2\pi} \int_{-\infty}^{\infty} e^{i\,k\,x}\, dk \int_{-\infty}^{\infty} u(r,t)\, e^{-i\,k\,r}\, dr\,. \tag{15}$$

The more general conditions under which the equality in the repeated integral in Eq. 15 holds depend upon the regularity assumptions imposed upon the function u.[†] Other useful formulae that will be used in subsequent sections include the space-shifting property:

$$\mathcal{F}\{f(x - x_0) : x \to k\} = \widehat{f}(k) e^{-i\,k\,x_0}\,, \tag{16}$$

---

*All functions u considered in this work are $u \in L^1(\mathbb{R}) \cap L^2(\mathbb{R})$ for example, $\frac{1}{1+x^2}$, $\frac{2}{\sqrt{2\pi}} e^{-2x^2}$, $e^{-x} H(x)$; however, there are functions u that are absolutely integrable $\int_{-\infty}^{\infty} |u|\, dx < +\infty$ but not square integrable $\int_{-\infty}^{\infty} |u|^2\, dx < +\infty$ and vice versa, see for example, pg. 306 of Weinberger.[18]

[†]For example, Eq. 15 can be derived by applying the Abel Limit definition,[19]

$$\int_{-\infty}^{\infty} f(k)\, dk := \lim_{\delta \to 0^+} \int_{-\infty}^{\infty} e^{-\delta |k|} f(k)\, dk\,,$$

to the first integral in Eq. 15.

the n^{th} derivative property, if $f(x)$ and its first n derivatives are continuous for all real values of x[‡],

$$\mathcal{F}\{f^n(x) : x \to k\} = (i\,k)^n \widehat{f}(k)\,, \tag{17}$$

and the convolution (or Faltung) property,

$$\begin{aligned} &\mathcal{F}\{f * h\}(x) = \mathcal{F}\{f\} \cdot \mathcal{F}\{h\} = \widehat{f} \cdot \widehat{h}\,, \\ &\text{or,} \quad f * h = \mathcal{F}^{-1}(\widehat{f} \cdot \widehat{h}) = \int_{-\infty}^{\infty} f(k)\, h(x-k)\, dk\,, \\ &\text{and,} \quad f * h = h * f\,, \end{aligned} \tag{18}$$

where "$*$" denotes convolution and "$\cdot$" multiplication; in some instances, the latter property given by Eq. 18_2 will prove useful for constructing the IVP solutions by replacing the inverse Fourier transform operator by a convolution operator.

3.1 Fourier Transform of the Governing Equations

On taking the Fourier transform of the body-force-free version of the linear momentum balance in Eq. 1 we obtain (see also Eq. 19 of Weckner and Abeyaratne[5])

$$\frac{\partial^2 \widehat{u}(k,t)}{\partial t^2} \,+\, \omega^2(k)\, \widehat{u}(k,t) \,=\, 0\,, \tag{19}$$

and the Fourier transform of the initial conditions, given by Eq. 3 results in,

$$\widehat{u}(k,0) = \widehat{f}(k) = \int_{-\infty}^{\infty} u(x,0)\, e^{-i\,k\,x}\, dx, \quad \widehat{\dot{u}}(k,0) = \widehat{g}(k) \,=\, \int_{-\infty}^{\infty} \dot{u}(x,0)\, e^{-i\,k\,x}\, dx\,. \tag{20}$$

The general nonlocal IVP solution $\widehat{u}(k,t)$ to differential Eq. 19 for the displacement in the Fourier transform domain is

$$\widehat{u}(k,t) \,=\, \widehat{A}(k)\, e^{i\,\omega(k)\,t} \,+\, \widehat{B}(k)\, e^{-i\,\omega(k)\,t}\,, \tag{21}$$

where the nonlinear dispersion relation $\omega(k)$ is defined by integral Eq. 5 and func-

[‡]The consequences of applying the n^{th} derivative property to a function $f(x)$ that is only piecewise continuous and piecewise smooth are addressed in Appendixes E and F.

tions $\widehat{A}(k)$ and $\widehat{B}(k)$ are determined from the initial conditions (Eq. 20) to be,

$$\widehat{A}(k) \,=\, \frac{1}{2}\left(\widehat{u}(k,0) \,-\, i\,\frac{\widehat{\dot{u}}(k,0)}{\omega(k)}\right) \quad \text{and} \quad \widehat{B}(k) \,=\, \frac{1}{2}\left(\widehat{u}(k,0) \,+\, i\frac{\widehat{\dot{u}}(k,0)}{\omega(k)}\right). \tag{22}$$

On substituting Eq. 22 into the nonlocal Fourier transform domain solution in Eq. 21 and simplifying we find that,

$$\widehat{u}(k,t) \,=\, \widehat{u}(k,0)\,\cos(\omega(k)\,t) \,+\, \frac{\widehat{\dot{u}}(k,0)}{\omega(k)}\,\sin(\omega(k)\,t)\,. \tag{23}$$

On taking the inverse Fourier transform of Eq. 23, and using the definition given by Eq. 14, results in the most general form of the nonlocal displacement solution $u(x,t)^*$ in terms of the Fourier transforms of the initial displacement $\widehat{u}(k,0)$, particle velocity $\widehat{\dot{u}}(k,0)$ and dispersion relation $\omega(k)$,

$$u(x,t) \,=\, \frac{1}{2\pi}\int_{-\infty}^{\infty}\Big(\widehat{u}(k,0)\,\cos(\omega(k)\,t) \,+\, \frac{\widehat{\dot{u}}(k,0)}{\omega(k)}\,\sin(\omega(k)\,t)\Big)e^{i\,k\,x}\,dk\,. \tag{24}$$

The general solution given by Eq. 21 is analogous to the Laplace transform domain solution for waves in linear viscoelastic media under impact (cf., Eq. 53 of Gazonas et al.[9]); the functions $\Omega(s)$ that appear in the exponentials of the Laplace transform domain solution are related to the Carson transform of the relaxation modulus, and are analogous to the nonlinear dispersion relation $\omega(k)$ that appear in Eq. 21.

In an analogous fashion, on taking the Fourier transform of the body-force-free version of the linear momentum balance Eq. 2 for the local elastic medium we obtain,

$$\frac{\partial^2\widehat{u}_l(k,t)}{\partial t^2} \,+\, \omega^2(k)\,\widehat{u}_l(k,t) \,=\, 0\,. \tag{25}$$

In the general solution $\widehat{u}_l(k,t)$ to the classical local IVP, the dispersion relation is linear in the wavenumber, $\omega(k) \,=\, \omega \,=\, c\,k$:

$$\widehat{u}_l(k,t) \,=\, \widehat{A}(k)\,e^{i\,\omega\,t} \,+\, \widehat{B}(k)\,e^{-i\,\omega\,t}\,, \tag{26}$$

*It turns out that our solution given by Eq. 24 can be transformed into Weckner and Abeyaratne's[5] result using convolution properties Eq. $18_{2,3}$; see for example, their Eq. 21 given by $u(x,t) \,=\, \int_{-\infty}^{\infty}\Big(u_0(x-\widehat{x})\,\dot{g}(\widehat{x},t) + v_0(x-\widehat{x})\,g(\widehat{x},t)\Big)\,d\widehat{x}$, where $g(x,t) \,=\, \mathcal{F}^{-1}\Big(\frac{\sin(\omega(k))\,t}{\omega(k)}\Big)$ is the Green's function for Eq. 1.

and the wave speed c is not dependent on frequency as is the case for dispersive media. On applying the initial conditions in Eq. 20 to the general local solution in Eq. 26 we find that,

$$\widehat{u}_l(k,t) \;=\; \widehat{u}_l(k,0)\,\cos(\omega\,t) \;+\; \frac{\widehat{\dot{u}}_l(k,0)}{\omega}\,\sin(\omega\,t)\,. \tag{27}$$

On taking the inverse Fourier transform of Eq. 27 and using the definition given by Eq. 14 results in,

$$\begin{aligned} u_l(x,t) \;&=\frac{1}{2\pi}\int\limits_{-\infty}^{\infty}\Big(\widehat{u}_l(k,0)\,\cos(\omega\,t) \;+\; \frac{\widehat{\dot{u}}_l(k,0)}{\omega}\,\sin(\omega\,t)\Big)e^{i\,k\,x}\;dk\,, \\ &=\mathcal{F}^{-1}\{\widehat{u}_l(k,t)\}\,. \end{aligned} \tag{28}$$

3.1.1 A Correspondence Principle

It is thus evident that for solution of nonlocal microelastic peridynamic IVPs on an infinite domain, we can use a **correspondence principle**,* stated here without proof, to obtain the Fourier transformed nonlocal peridynamic solution given by Eq. 21 after having first determined the Fourier transformed local elastic solution given by Eq. 26, namely,

$$\widehat{u}(\omega,t) = \widehat{u}_l(\omega(k),t)\,. \tag{29}$$

This local-nonlocal correspondence principle is similar to that used to obtain dynamic viscoelastic solutions (involving convolutions in time) to the wave equation from elastic solutions using Fourier transform (cf., Eq. 53 of Carcione et al.[21])† or Laplace transform methods.[22,23] Our ability to obtain solutions depends upon whether we can find analytical or numerical inverse Fourier transforms of Eq. 29. The local-nonlocal correspondence principle, as stated, only requires identification of a dispersion relation, possibly from experimentation, and does not require identification of a micromodulus function, although the latter is implicitly defined via integral Eq. 5.

*This correspondence principle is not related to the concept of a correspondence material model,[20] "which defines what it means to require a peridynamic material model to agree with a given classical material model for a given deformation."

†Carcione et al.[21] simply replace the real wave number in the elastic solution by the complex wave number to obtain the viscoelastic solution.

4. Solution of the Initial Value Problems

In this section, we solve four IVPs considered in Examples 5.1 and 5.2 of Beyer et al.[1] for problems that involve both local and nonlocal (peridynamic) wave equations for both continuous and discontinuous initial data; for brevity we only study problems in which $u(x,0) \neq 0$ and $\dot{u}(x,0) = 0$. The initial conditions in the next two example problems 1 and 2 are *continuous*.

4.1 Problem 1: Local Wave Equation with Continuous Initial Conditions

The initial condition and its Fourier transform for Problem 1 are given by,

$$\begin{aligned} u_l(x,0) = f(x) = \frac{1}{1+x^2}\,, \quad \dot{u}_l(x,0) = 0\,, \\ \implies \widehat{u}_l(k,0) = \widehat{f}(k) = \pi e^{-|k|}\,, \quad \widehat{\dot{u}}_l(x,0) = 0\,. \end{aligned} \tag{30}$$

On substituting the Fourier transformed initial conditions Eq. 30_2 into Eq. 28, we arrive at the local solution for the displacements,

$$u_l(x,t) \;=\; \mathcal{F}^{-1}\widehat{u}_l(k,t) \;=\; \frac{1}{2\pi}\int\limits_{-\infty}^{\infty} \pi\, e^{-|k|}\, \cos\big(\omega\, t\big)\, e^{i\,k\,x}\, dk\,, \quad \omega = k\,c\,. \tag{31}$$

On applying the convolution property Eq. 18_2 to Eq. 31 we find that:

$$u_l(x,t) = \int\limits_{-\infty}^{\infty} f(y)\, h(x-y,t)\, dy\,, \tag{32}$$

where,

$$f(y) \;=\; \frac{1}{1+y^2}\,, \tag{33}$$

is the initial condition Eq. 30_1 and,

$$h(x,t) \;=\; \frac{1}{2\pi}\int\limits_{-\infty}^{\infty} e^{i\,k\,x}\, \cos\big(k\,c\,t\big)\, dk \;=\; \frac{1}{2}(\delta(ct+x) + \delta(ct-x))\,. \tag{34}$$

On substituting Eqs. 33 and 34 into Eq. 32 we obtain the following expression:

$$u_l(x,t) \;=\; \int_{-\infty}^{\infty} \frac{1}{1+y^2}\,\frac{1}{2}(\delta(ct+(x-y)) + \delta(ct-(x-y)))\, dy\,. \tag{35}$$

On using the "sifting" property[24] of the Dirac delta δ function to Eq. 35 we arrive at the explicit local solution:

$$u_l(x,t) \;=\; \frac{1}{2\,(1+(ct+x)^2)} + \frac{1}{2\,(1+(-ct+x)^2)}\,. \tag{36}$$

Alternatively, the same solution can be obtained by applying the space-shifting property (Eq. 16) to Eq. 26 we find that:

$$\begin{aligned}
u_l(x,t) &= \mathcal{F}^{-1}\widehat{u}_l(k,t) = \mathcal{F}^{-1}\Big\{\frac{\widehat{f}(k)}{2}\,e^{i\,k\,c\,t}\Big\} \;+\; \mathcal{F}^{-1}\Big\{\frac{\widehat{f}(k)}{2}\,e^{-i\,k\,c\,t}\Big\}\;, \text{or,}\\
u_l(x,t) &= \frac{1}{2}f(x\;+\;c\,t) + \frac{1}{2}f(x\;-\;c\,t)\,, \qquad (37)\\
u_l(x,t) &= \frac{1}{2}\left(\frac{1}{1+(x\;+\;c\,t)^2} + \frac{1}{1\;+\;(x\;-\;c\,t)^2}\right)\;,
\end{aligned}$$

which is the D'Alembert solution obtained by a more direct method. The function f in Eq. 37_2 is given by the initial condition Eq. 30_1, and thus one can see that Eqs. 37_3 and 36 are equivalent.

4.1.1 Problem 1a: Nonlocal Wave Equation with Continuous Initial Conditions

Beyer et al.[1] do not solve* the nonlocal version of Problem 1 but we can use the local-nonlocal correspondence principle (Eq. 29) to transform the local solution (Eq. 31) to the nonlocal solution,

$$u(x,t) \;=\; \mathcal{F}^{-1}\widehat{u}(k,t) \;=\; \frac{1}{2\pi}\int\limits_{-\infty}^{\infty} \pi\,e^{-|k|}\,\cos\big(\omega(k)\,t\big)\,e^{i\,k\,x}\,dk\,, \tag{38}$$

where here, and in what follows, we use the nonlocal dispersion relation Eq. 8 so that we may directly compare our IVP solutions with those of Beyer et al.[1]

*The Beyer et al.[1] IVP solutions are written in terms of an infinite series of spherical Bessel functions of the first kind, and constructed through determination of the $k^{th}-$convolution of the micromodulus function with the initial condition (either displacement or velocity); using this method we were unable to derive a nonlocal series solution to Problem 1 because of the inherent difficulty in forming the $k^{th}-$convolution of the micromodulus function with this particular displacement initial condition given by Eq. 30.

4.2 Problem 2: Nonlocal Wave Equation with Continuous Initial Conditions

The initial condition and its Fourier transform for Problem 2 are given by,

$$\begin{aligned} u(x,0) = f(x) &= \frac{2}{\sqrt{2\pi}} e^{-2\,x^2}\,, \quad \dot{u}(x,0) = 0\,, \\ \implies \widehat{u}(k,0) = \widehat{f}(k) &= e^{-\frac{k^2}{8}}\,, \qquad\qquad \widehat{\dot{u}}(x,0) = 0\,. \end{aligned} \tag{39}$$

On substituting the Fourier transformed initial conditions in Eq. 39_2 and the nonlinear dispersion relation from Beyer et al.[1] (Eq. 8) into Eq. 24, results in the solution to the nonlocal IVP,

$$u(x,t) \;=\; \mathcal{F}^{-1}\widehat{u}(k,t) \;=\; \frac{1}{2\pi}\int\limits_{-\infty}^{\infty} e^{-\frac{k^2}{8}}\,\cos\left(\sqrt{1\,-\,e^{-\frac{k^2}{2}}}\;t\right) e^{i\,k\,x}\,dk\,. \tag{40}$$

Equation 40 cannot be integrated in closed form but will be numerically integrated using Mathematica's NIntegrate function as well as using an IFFT algorithm in a subsequent section. The Beyer et al.[1] solution* to this problem is given by,

$$u(x,t) \;=\; \sqrt{\frac{2}{\pi}}\sum_{k=0}^{\infty}\frac{(\sqrt{\frac{\mathbf{c}\,t^2}{\rho}})^{k+1}}{2^k k!} j_{k-1}(\sqrt{\frac{\mathbf{c}\,t^2}{\rho}})\frac{e^{-\frac{2\,x^2}{1+4\,k}}}{\sqrt{1+4\,k}}\,, \tag{41}$$

where j_{k-1} is the spherical Bessel function of the first kind.

An error estimate ϵ for the sum involving $N-$ terms in Eq. 41 is determined using $\epsilon \;\approx\; \frac{\pi}{N!}\,e^{\frac{t^2}{4}}$, where t is the time (cf., Corollary 4.6. (Error Estimates) in Beyer et al.[1]). For example, for $t \;=\; 20$ and $N \;=\; 50$ terms the error in the "exact" solution given by Eq. 41 is $\epsilon \;\approx\; 2.78 \times 10^{-21}$. The initial conditions in the next two example problems 3 and 4 are *discontinuous*.

*Here we integrate Eq. 9 to obtain the positive constant $\mathbf{c} \;:=\; \int\limits_{\mathbb{R}} C(\xi)d\xi \;=\; 1$ that appears in Eqs. 41 and 46, cf., pg. 25 of Beyer et al.[1]; note also that $\mathbf{c} \;\neq\; c$, that is, the wave speed.

4.3 Problem 3: Local Wave Equation with Discontinuous Initial Conditions

The initial condition and its Fourier transform for Problem 3 are given by,

$$\begin{aligned} u(x,0) = f(x) = e^{-x}\,H(x)\,, \quad & \dot{u}(x,0) = 0\,, \\ \implies \widehat{u}(k,0) = \widehat{f}(k) = \frac{1-i\,k}{1+k^2}\,, \quad & \widehat{\dot{u}}(x,0) = 0\,. \end{aligned} \tag{42}$$

On substituting the Fourier transformed initial conditions Eq. 42_2 into Eq. 28 we arrive at the local solution which can be integrated in closed form as,

$$\begin{aligned} u_l(x,t) \;&=\; \mathcal{F}^{-1}\widehat{u}_l(k,t) \;=\frac{1}{2\pi}\int\limits_{-\infty}^{\infty}\frac{1-i\,k}{1+k^2}\,\cos\big(\omega\,t\big)\,e^{i\,k\,x}\,dk\,, \quad \omega = k\,c\,, \\ &=\;\frac{1}{2}\,e^{-(x\,+\,c\,t)}\,H(x\,+\,c\,t)\,+\,\frac{1}{2}\,e^{-(x\,-\,c\,t)}\,H(x\,-\,c\,t)\,. \end{aligned} \tag{43}$$

This is the D'Alembert solution that can also be obtained by the standard method through evaluation of the function f in Eq. 42_1 at $x \;\rightarrow\; x \,\pm\, c\,t$ as was done previously in Eq. 37_2.

4.4 Problem 4: Nonlocal Wave Equation with Discontinuous Initial Conditions

The initial condition and its Fourier transform for Problem 4 are given by,

$$\begin{aligned} u(x,0) = f(x) = e^{-x}\,H(x)\,, \quad & \dot{u}(x,0) = 0\,, \\ \implies \widehat{u}(k,0) = \widehat{f}(k) = \frac{1-i\,k}{1+k^2}\,, \quad & \widehat{\dot{u}}(x,0) = 0\,. \end{aligned} \tag{44}$$

On applying the local-nonlocal correspondence principle by substituting the nonlinear dispersion relation Eq. 8 into Eq. 43_1 we obtain the solution to the nonlocal IVP,

$$u(x,t) \;=\; \mathcal{F}^{-1}\widehat{u}(k,t) \;=\; \frac{1}{2\pi}\int\limits_{-\infty}^{\infty}\frac{1-i\,k}{1+k^2}\,\cos\big(\sqrt{1\,-\,e^{-\frac{k^2}{2}}}\;t\big)\,e^{i\,k\,x}\,dk\,. \tag{45}$$

Equation 45 cannot be integrated in closed form but will be numerically integrated using Mathematica's NIntegrate function as well as an IFFT algorithm in a subse-

quent section. The Beyer et al. solution[1] to this problem is given by,

$$
\begin{aligned}
u(x,t) \; &= \cos(\sqrt{\frac{\mathbf{c}\,t^2}{\rho}})\, e^{-x}\, H(x) \\
&+ \frac{2}{\pi} \sum_{k=1}^{\infty} \frac{(\sqrt{\frac{\mathbf{c}\,t^2}{\rho}})^{k+1}}{2^k\, k!}\, j_{k-1}(\sqrt{\frac{\mathbf{c}\,t^2}{\rho}})\, e^{\frac{k}{2}-x}\, \text{erfc}\left(\frac{k\,-\,x}{\sqrt{2\,k}}\right) ,
\end{aligned}
\tag{46}
$$

where H and erfc denote the Heaviside step and complementary error functions, respectively.

5. Numerical Solution of the Initial Value Problems

In this section, we illustrate the solutions to the initial value problems posed in Section 4 by employing Mathematica's NIntegrate function and the IFFT algorithm developed in this report; the accuracy of our numerical solutions are quantified using the absolute error (AE), which is plotted at each discrete time instant and spatial location, as well as the absolute timing (AT), in seconds, required for each solution method; these quantities appear in Table 1 at the end of Section 5.

The AE is defined for every point (t, x) in the computational domain denoted by indices (i, j),

$$
AE(i,j) = |u_{exact}(i,j) - u_{num}(i,j)| \,, \tag{47}
$$

where $u(i, j)$ is the displacement and the subscript num refers to the numerical solutions. In the figures that follow the L^∞-norm of the absolute error $||AE(i,j)||_\infty$ given by Eq. 47 is shown as the maximum value of the ordinate in the plots, so that solution accuracy can be directly compared between Mathematica's NIntegrate function and the IFFT algorithm (see also Table 1).* The relative error was not used as an error measure since the solutions involving jump discontinuities pass through zero, and the relative error is undefined in these portions of the domain cf., Problems 3 and 4 are illustrated in Figs. 8 and 10, respectively. Alternatively, we could have normalized $AE(i,j)$ by $||u_{exact}(i,j)||_\infty$ but this latter quantity is unity for the initial conditions given in Problems 1, 2, and 4 studied in this report and thus would not alter the magnitude of this latter normalized error measure.

*In the remainder of this report, for clarity, the orange-colored figures refer to solutions obtained using the Mathematica's NIntegrate function, the yellow-colored figures refer to solutions using the IFFT algorithm, and the cyan-colored figure refers to the series solution.

For determining accuracy in our solutions using the previous error measures, either the exact analytical solutions are used or "exact" series solutions.[1] As mentioned previously, the error estimate ϵ for the sum involving $N-$ terms in Eq. 41 is estimated using $\epsilon \approx \frac{\pi}{N!} e^{\frac{t^2}{4}}$, where t is the time (cf., Corollary 4.6. (Error Estimates) in Beyer et al.[1]). For example, for $t = 20$ and $N = 50$ terms the error in the "exact" series solution given by Eq. 41 is $\epsilon \approx 2.78 \times 10^{-21}$.

All calculations use the parallel capabilities inherent in Mathematica's built-in functions and are performed on a desktop system with an Intel (R) Xeon (R) Gold 6136 CPU running at 3.00 GHz and 48 logical processors and 256 GB RAM. These calculations are conducted at a minimum of machine precision where $MachinePrecision = 15.9546 decimal digits of precision for floating point calculations.

5.1 Aliasing in Spatial and Frequency Domains

In order to implement the IFFT algorithm in Mathematica the spatial domain is discretized using,

$$Dv = \frac{2\,\pi}{n\,dk}\,, \tag{48}$$

where Dv is the spatial resolution, $n = 2^{jj}$ is a power of two and dk is the spatial sampling period,

$$dk = \frac{1}{10^{\frac{kk}{2}-1}}\,, \tag{49}$$

with spatial discretization given by,

$$x_i \;=\; Dv * (i - n/2), \quad i \;=\; 1...n\,, \tag{50}$$

(see Mathematica source code in Appendix C). Figure 1 illustrates contours of the maximum absolute error using the IFFT algorithm vs. the exact local solution given by Eq. 36 with $c = 1$ as a function of jj and kk; a relative minimum in the error occurs for $jj = 14$ or $n = 2^{jj} = 16,384$ and $kk = 5$ or $dk = \frac{1}{10\sqrt{10}}$ so we use these values in all the IFFT solutions in the following sections. Thus for a fixed n we see that the choice of dk is a compromise between aliasing in frequency and aliasing in space.[25]

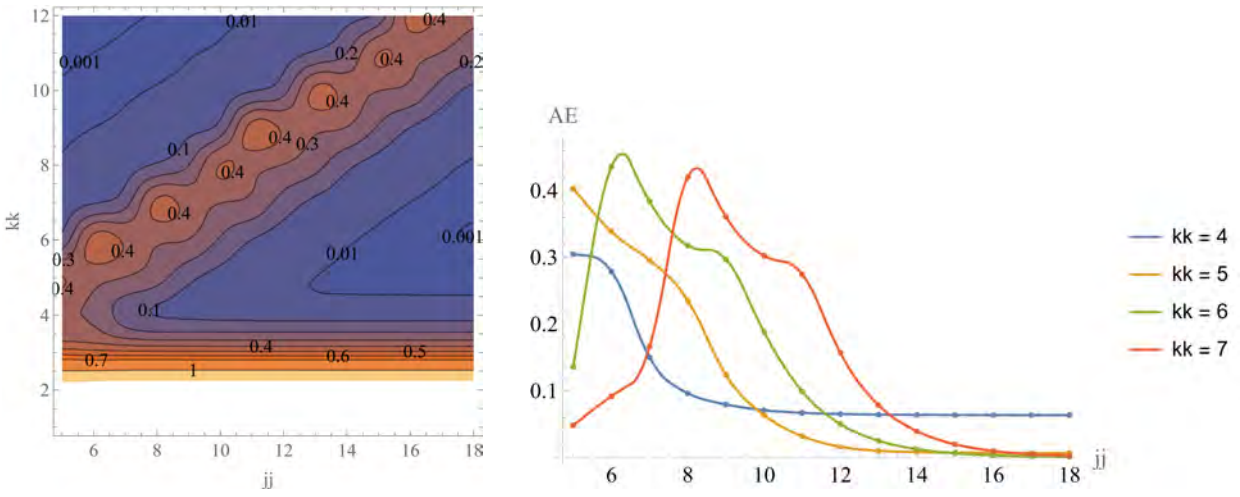

(a) (b)

Fig. 1 (a) Absolute error contour map as a function of jj and kk; (b) absolute error vs. jj for selected kk values

5.2 Problem 1: NIntegrate Solution and Absolute Error

Figure 2 shows the NIntegrate solution to Problem 1 and the associated AE.

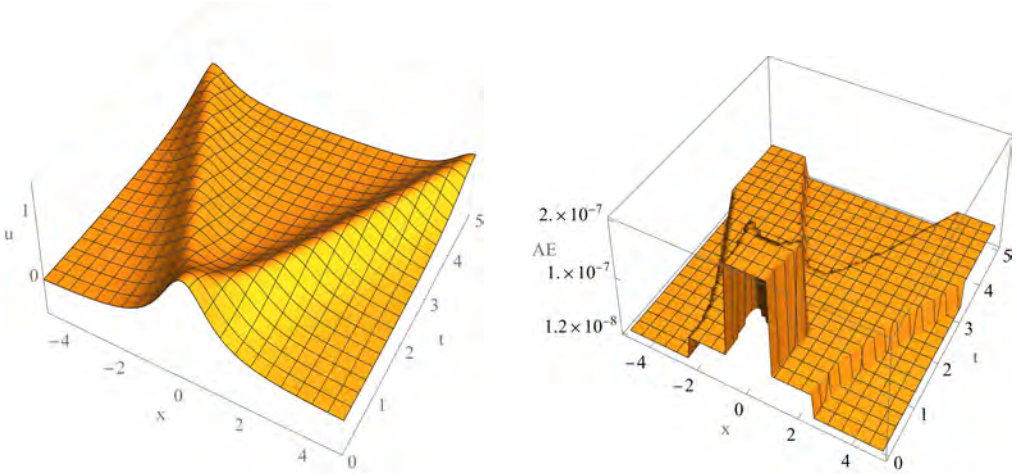

(a) (b)

Fig. 2 Problem 1: (a) Numerical solution by integration of Eq. 31 using Mathematica's[7] NIntegrate function; (b) AE $=$ |exact $-$ numerical|; the exact solution is given by Eq. 37$_2$

5.3 Problem 1: IFFT Solution and Absolute Error

Figure 3 shows the IFFT solution to Problem 1 and the associated AE.

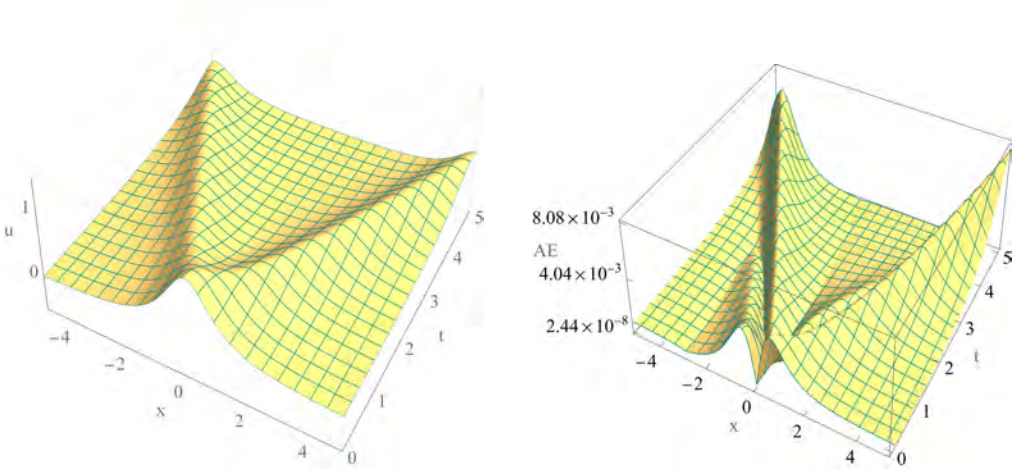

(a) (b)

Fig. 3 Problem 1: (a) Numerical solution by IFFT of Eq. 31 using Mathematica's[7] Inverse-Fourier function; (b) AE $=$ |exact $-$ numerical|; the exact solution is given by Eq. 37$_2$

5.4 Problem 1a: NIntegrate and IFFT Solutions

Figure 4 shows the NIntegrate and IFFT solutions to Problem 1a.

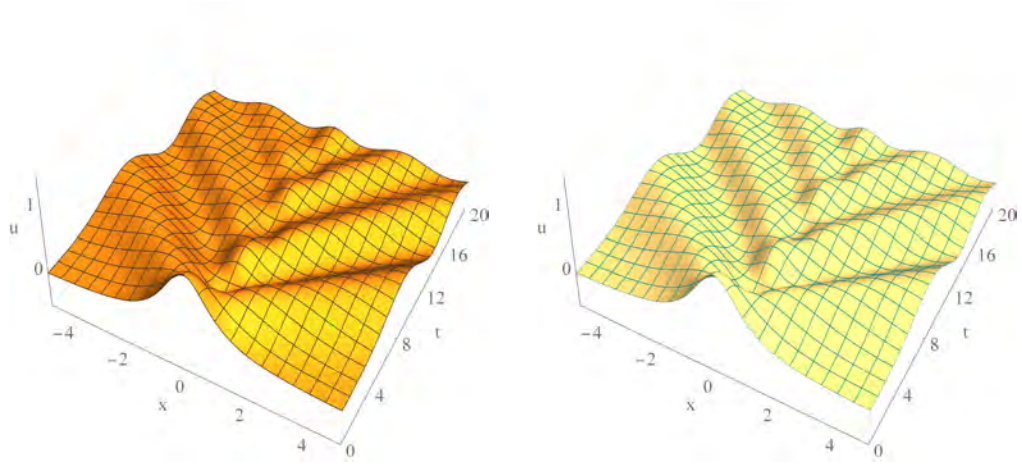

(a) (b)

Fig. 4 Problem 1a: (a) Numerical solution by integration of Eq. 38 using Mathematica's[7] NIntegrate function; (b) Numerical solution by IFFT of Eq. 38 using Mathematica's[7] Inverse-Fourier function; an AE plot is not generated here, because there is no exact solution to this problem

5.5 Problem 2: NIntegrate Solution and Absolute Error

Figure 5 shows the NIntegrate solution to Problem 2 and the associated AE.

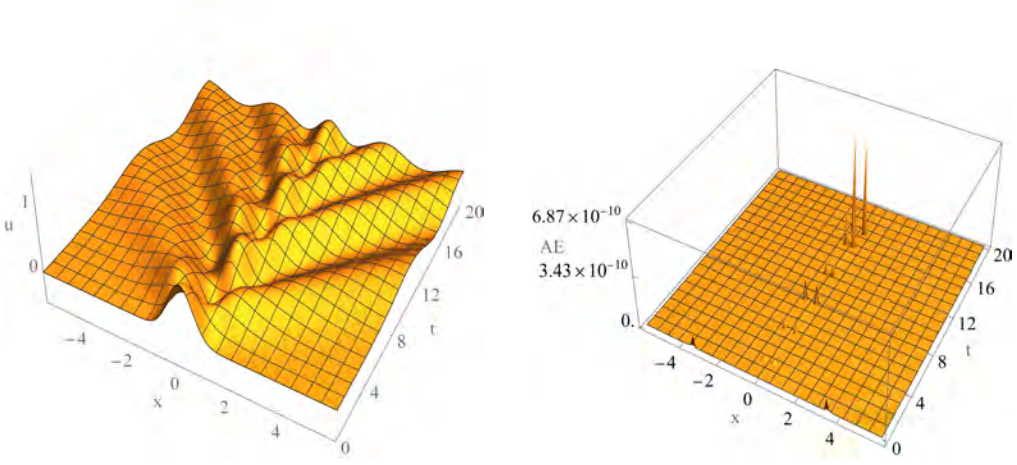

(a) (b)

Fig. 5 Problem 2: (a) Numerical solution by integration of Eq. 40 using Mathematica's[7] NIntegrate function; (b) AE $=$ |exact $-$ numerical|; the exact solution is given by Eq. 41

5.6 Problem 2: IFFT Solution and Absolute Error

Figure 6 shows the IFFT solution to Problem 2 and the associated AE.

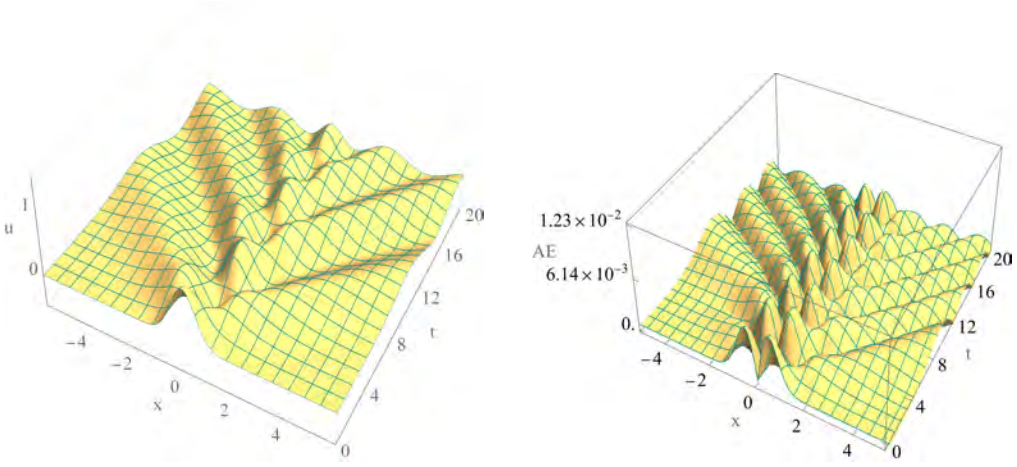

(a) (b)

Fig. 6 Problem 2: (a) Numerical solution by IFFT of Eq. 40 using Mathematica's[7] Inverse-Fourier function; (b) AE $=$ |exact $-$ numerical|; the exact solution is given by Eq. 41

5.7 Problem 3: NIntegrate Solution and Absolute Error

Figure 7 shows the NIntegrate solution to Problem 3 and the associated AE.

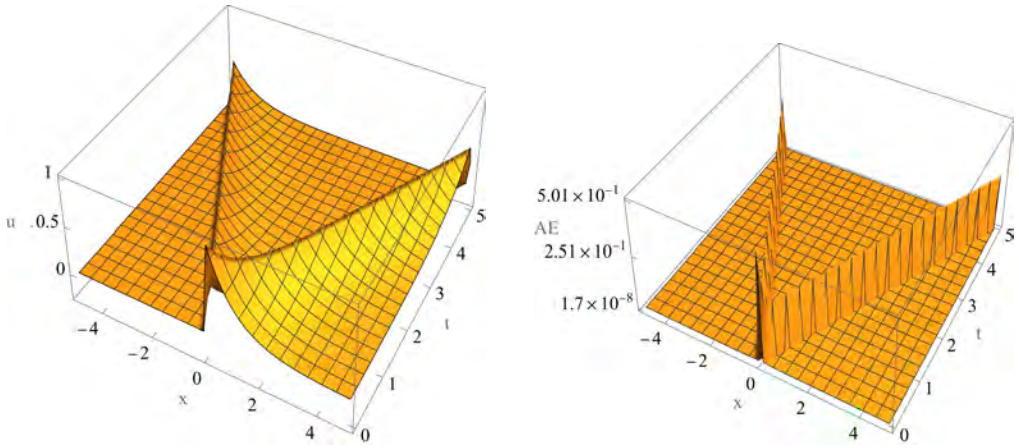

(a) (b)

Fig. 7 Problem 3: (a) Numerical solution by integration of Eq. 43_1 **using Mathematica's[7] NIntegrate function; (b) AE** $=$ **|exact** $-$ **numerical|; the exact solution is given by Eq.** 43_2

5.8 Problem 3: IFFT Solution and Absolute Error

Figure 8 shows the IFFT solution to Problem 3 and the associated AE.

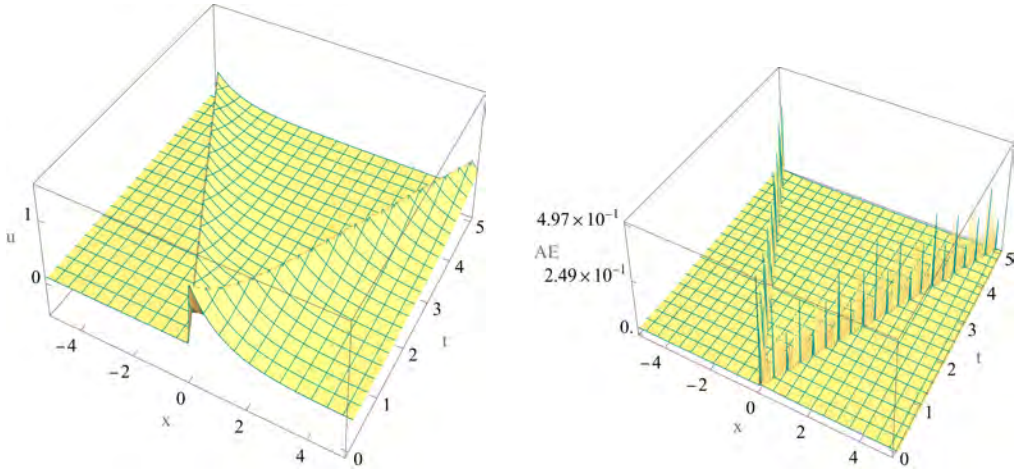

(a) (b)

Fig. 8 Problem 3: (a) Numerical solution by IFFT of Eq. 43 **using Mathematica's[7] Inverse-Fourier function; (b) AE** $=$ **|exact** $-$ **numerical|; the exact solution is given by Eq.** 43_2

5.9 Problem 4: NIntegrate Solution and Absolute Error

Figure 9 shows the NIntegrate solution to Problem 4 and the associated AE.

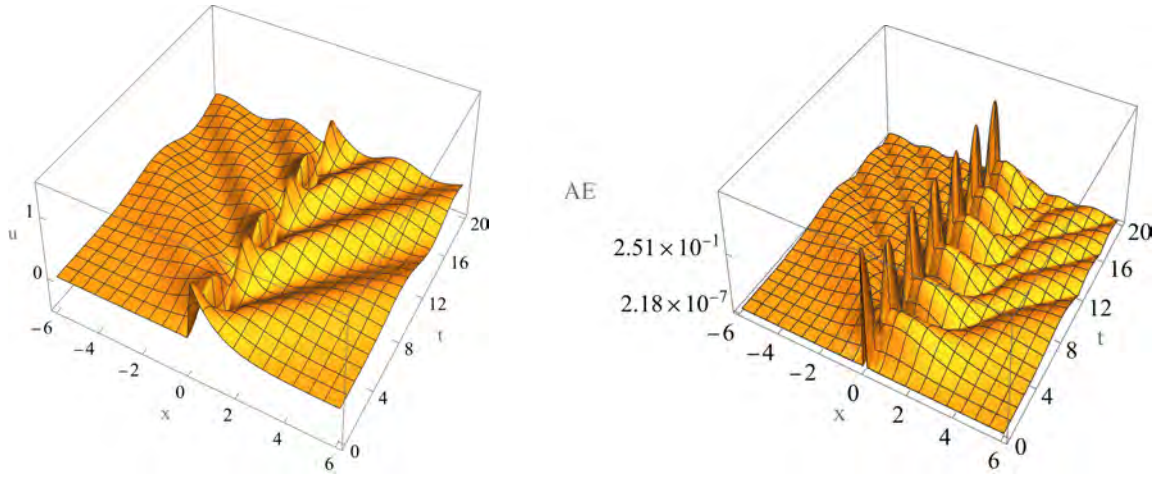

(a) (b)

Fig. 9 Problem 4: (a) Numerical solution by integration of Eq. 45_1 **using Mathematica's[7] NIntegrate function; (b) AE** $=$ **|exact** $-$ **numerical|; the exact solution is given by Eq.** 46

5.10 Problem 4: IFFT Solution and Absolute Error

Figure 10 shows the IFFT solution to Problem 4 and the associated AE.

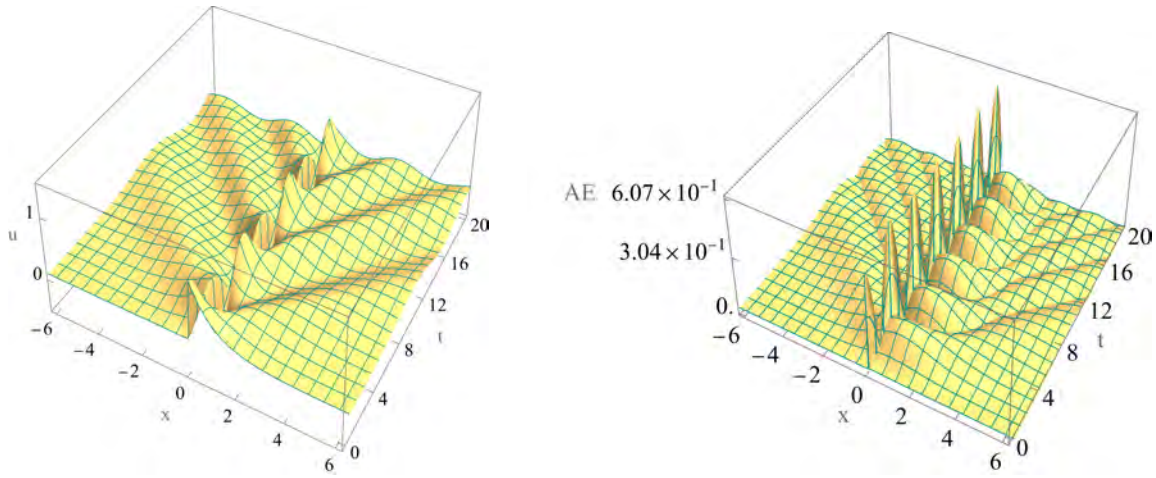

(a) (b)

Fig. 10 Problem 4: (a) Numerical solution by IFFT of Eq. 45_1 **using Mathematica's[7] Inverse-Fourier function; (b) AE** $=$ **|exact** $-$ **numerical|; the exact solution is given by Eq.** 46

6. Discussion

It is evident from Table 1 that both NIntegrate functions using the DoubleExponential Method and the IFFT algorithm produce solutions for Problems 1 and 2 requiring less than 1 min of CPU time with NIntegrate providing more accurate solutions than the IFFT algorithm; for these two problems, the initial condition was continuous. However, Beyer et al.[1] do not solve Problem 1 with the initial condition given by Eq. 30_1 and we were unable to accomplish this, but instead applied our correspondence principle to solve this nonlocal problem using both the NIntegrate function and the IFFT algorithm, which appear in Fig. 4.

Problems 3 and 4 involve initial conditions with displacement jump discontinuities at the origin $x = 0$, that is they are discontinuous and given by Eq. 42_1. Although not all jump discontinuities have physical relevance, we may think of the jump discontinuity in displacement as representing an initial "fracture" of the 1-D local continuum at the origin. Indeed, such displacement discontinuity functions appear in the integrand of finite part integrals for solution of crack boundary value problems. Interestingly, the displacement discontinuity for the local problem immediately heals at $x = 0\,, t = 0^+$, and can be seen propagating away from the origin at wave speed $c = 1$ into the undisturbed local medium towards $x = \pm\infty$, cf., Figs. 7 and 8, which correspond to the NIntegrate and IFFT solutions to this problem, respectively. Both solutions contain absolute errors of comparable magnitude that are maximum in the neighborhood of the displacement jump. In fact, the IFFT solution errors at the jump discontinuities that appear in Figs. 8 and 10 are consistent with "INVERSION THEOREM 2." on pg. 317 of Weinberger,[18] which states that if $u(x,t)$ has a jump discontinuity at x_0 then the inversion formula gives a solution which is the *average of the jump magnitude* at the discontinuity,

$$\frac{1}{2}\left(u\left(x_0+0,t\right)+u\left(x_0-0,t\right)\right)=\frac{1}{2\,\pi}\lim_{L\to\infty}\int_{-L}^{L}\widehat{u}(k,t)e^{-ikx_0}\,dk\,. \tag{51}$$

Furthermore, since the local IVP solution $u_l(x,t)$ given by Eq. 43_2 is piecewise continuous, the value that the displacement function $u_l(x,t)$ takes on depends upon which of the one-sided limits is employed in its evaluation, that is, either from above or below; as such, the particular values that $u_l(x,t)$ takes on at the jump discontinuity have no real physical significance. A more detailed discussion of the propagation of discontinuities in stress and particle velocity induced by impact can be found

in Gazonas et al.[26] For Problems 3 and 4 that involve initial conditions with displacement jump discontinuities, Mathematica's NIntegrate function using the DoubleExponential Method did not converge to a solution, and thus we employed the GaussKronrodRule as a method that converged only on the finite transform domain $k \in \{-300, 300\}$; increasing the size of this domain resulted in severe numerical underflow errors and unacceptable computation times. Even using the GaussKronrodRule, the solution to Problem 4. required a surprising 3.63 h of CPU time on 48 processors, (see Table 1).

In contrast, the nonlocal solutions to this same problem that appear in Figs. 9 and 10 have displacement jump discontinuities that remain stationary at the origin (i.e., do not heal), and are thus more physically satisfying than the local solutions that continuously fracture the 1-D medium through propagation along characteristics. For the nonlocal solutions, even though the discontinuities remain stationary at the origin, waves continuously propagate away from the source of the discontinuity, which for a peridynamic medium is not a fracture unless (e.g.), a critical stretch or other failure criterion is satisfied. Jump displacement discontinuities, which become negative at times $t = 0^+$, cf., Problem 4 and illustrated in Figs. 9 and 10, indicate that particle interpenetration occurs if the displacement is considered to be longitudinal. However, as pointed out by Weckner and Abeyeratne[5] this is not problematic if the displacement jump is considered to be transverse. Finally, the appearance of stationary jump discontinuities is not a new phenomenon, but has also been reported in solutions to IVPs for wave propagation in 1-D linear viscoelastic media.[27]

Table 1 The L^∞ norm of the Absolute Error and Absolute Timing for solutions to Problems 1-4

Problem no.: Method	No. of (x,t) grid points	$L^{\infty *}$	AT† (s)	k-range
Problem 1: NIntegrate‡	$(101, 51)$	2.00×10^{-7}	54	$(-\infty, \infty)$
Problem 1: InverseFourier§	$(2^{14}, 101)$	8.08×10^{-3}	23	$(-8192, 8192)$
Problem 2: NIntegrate	$(201, 121)$	6.87×10^{-10}	9	$(-\infty, \infty)$
Problem 2: InverseFourier	$(2^{14}, 201)$	1.23×10^{-2}	42	$(-8192, 8192)$
Problem 3: NIntegrate	$(101, 51)$	5.01×10^{-1}	58	$(-300, 300)$
Problem 3: InverseFourier	$(2^{14}, 101)$	4.97×10^{-1}	26	$(-8192, 8192)$
Problem 4: NIntegrate	$(201, 121)$	2.51×10^{-1}	$13,056$	$(-300, 300)$
Problem 4: InverseFourier	$(2^{14}, 201)$	6.07×10^{-1}	53	$(-8192, 8192)$

7. Solution of a Peridynamic IVP Using Dispersion Relations Derived from a Periodically Layered Medium

In this section, we show how nonlinear dispersion relations can be derived using Floquet theory for a periodic medium consisting of alternating layers of aluminum and 4.5-min epoxy, together with the correspondence principle (Eq. 29), to solve an IVP for a homogenized peridynamic medium. This solution is also compared with the series solution method of Beyer et al.[1] where it is first necessary to derive the micromodulus function from the nonlinear dispersion relation.

7.1 Band Structure of the Dispersion Relation

The band structure for a periodically layered medium of infinite extent can be analytically determined by invoking Floquet theory, which results in the following dispersion relation for a unit cell consisting of two components, cf., Eq. 23 of Lee and Yang,[29]

$$\begin{aligned} \cos(k\,d) = &\cos\left(\frac{d_f\,\omega}{c_f}\right)\cos\left(\frac{d_m\,\omega}{c_m}\right) \\ &- \frac{1}{2}\sin\left(\frac{d_f\,\omega}{c_f}\right)\sin\left(\frac{d_m\,\omega}{c_m}\right)\left(\frac{c_m\eta_f}{c_f\eta_m} + \frac{c_f\eta_m}{c_m\eta_f}\right), \end{aligned} \tag{52}$$

$^*L^\infty = \max_i |AE(i,j)|$

†This column uses Mathematica's AbsoluteTiming (AT) function[7] rounded to the nearest second.

‡Mathematica source code for the various NIntegrate functions used in the solution to Problems 1 through 4 can be found in Appendix A.

§Mathematica source code for the various IFFT functions[28] used in the solution to Problems 1 through 4 can be found in Appendix B.

where k is the wavenumber, ω is the angular frequency, $d = d_f + d_m$ is the period of the unit cell consisting of fiber fraction d_f, and matrix fraction d_m. The fiber wave speed, elastic modulus, and density are c_f, η_f, ρ_f, respectively, where $c_f = \sqrt{\eta_f/\rho_f}$ and the matrix wave speed, elastic modulus, and density are c_m, η_m, ρ_m, respectively, where $c_m = \sqrt{\eta_m/\rho_m}$. Using these definitions, together with the material properties for aluminum ($d_f = 0.09$ mm), and 4.5-min epoxy ($d_m = 0.02$ mm) from Table 1 of Esquivel-Sirvent and Cocoletzi[30] we can plot the frequency spectrum using the reduced zone scheme[29] illustrated in Fig. 11(a), which reproduces Fig. 2 of Esquivel-Sirvent and Cocoletzi.[30]

As mentioned in a previous section, the methodology described herein is not limited to a unit cell comprised of only two materials but can be extended to unit cells containing any number of sublayers of arbitrary length and material properties using the recursive dispersion relations derived by Velo et al.[15]

On applying Mathematica's "NonlinearModelFit" function[7] to the data points from the first pass band shown in Fig. 11(a) to the nonlinear dispersion relation,

$$\omega(k) = \sqrt{a\left(1 - e^{-\frac{1}{2}b^2k^2}\right)}\,, \tag{53}$$

we find "best-fit" parameters $a = 205.680$ and $b = 0.557383$; the fit to the data points from the first pass band is illustrated in Fig. 11(b). This nonlinear dispersion relation is consistent with a slight generalization of the micromodulus function used by Beyer et al.[1] and the dispersion relation given by Eq. 7 with $\rho = 1$, where a is proportional to the amplitude and $b = \sigma$ is the standard deviation of the Gaussian micromodulus function. This identification will allow us to directly compare the IVP solution using our IFFT method,

$$u(x,t) \;=\; \mathcal{F}^{-1}\widehat{u}(k,t) \;=\; \frac{1}{2\pi}\int_{-\infty}^{\infty} e^{-\frac{k^2}{8}} \cos\left(\sqrt{a\left(1 - e^{-\frac{1}{2}b^2k^2}\right)}\,t\right) e^{ikx}\,dk\,, \tag{54}$$

with the series solution,

$$u(x,t) \;=\; e^{-2x^2}\sqrt{\frac{2}{\pi}}\cos\left(\sqrt{a}t\right) + \sqrt{\frac{2}{\pi}}\sum_{k=1}^{\infty}\frac{(\sqrt{a}t)^{k+1} j_{k-1}\left(\sqrt{a}t\right) e^{-\frac{2x^2}{1+4kb^2}}}{(2^k k!)\sqrt{1+4kb^2}}\,. \tag{55}$$

The series solution shown in Eq. 55 was derived by first forming the k^{th}-convolution

of the micromodulus function $C(x) = \frac{a}{\sqrt{2\pi}b} e^{-\frac{x^2}{2b^2}}$ with initial condition $u(x,0) = \sqrt{\frac{2}{\pi}} e^{-2x^2}$. The solutions given by Eqs. 54 and 55 are illustrated in Fig. 13(a) and Fig. 13(b), respectively. The Mathematica source code for the IFFT solution appears in Appendix C and for the series solution in Appendix D.

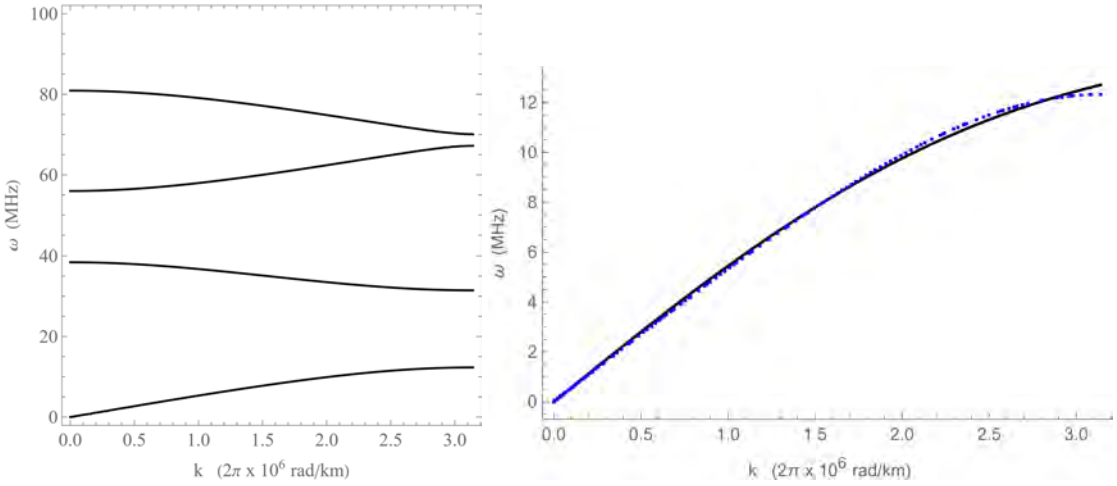

(a) (b)

Fig. 11 (a) Band structure of the dispersion relation in a periodically layered "superlattice" consisting of aluminum ($d_f = 0.09\,mm$) and 4.5-min epoxy ($d_m = 0.02\,mm$), with period $d = d_f + d_m$, reproduced from Fig. (2) of Esquivel-Sirvent and Cocoletzi[30] using Eq. 23 of Lee and Yang[29]; (b) Nonlinear least-squares fit to the first pass band in (a) using Mathematica's "NonlinearModelFit" function[7] applied to $\omega(k) = \sqrt{a\left(1 - e^{-\frac{1}{2}b^2k^2}\right)}$ with best fit parameters: $a = 205.680$ **and** $b = 0.557383$**.**

The nonlinear band structure of the dispersion relation generates waves that have different group and phase velocities whose magnitudes decrease as a function of frequency as illustrated in Fig. 12(a); Figure 12(b) shows how the group velocity varies with frequency for the first four pass bands determined using the frequency spectrum plotted using the extended zone scheme, cf., Fig. 2 of Lee and Yang[29] and how the group velocity can be determined from the phase velocity using Eq. 20-15 from Pilant[31] or Eq. 3.85 from Ben-Menahem and Singh.[32]

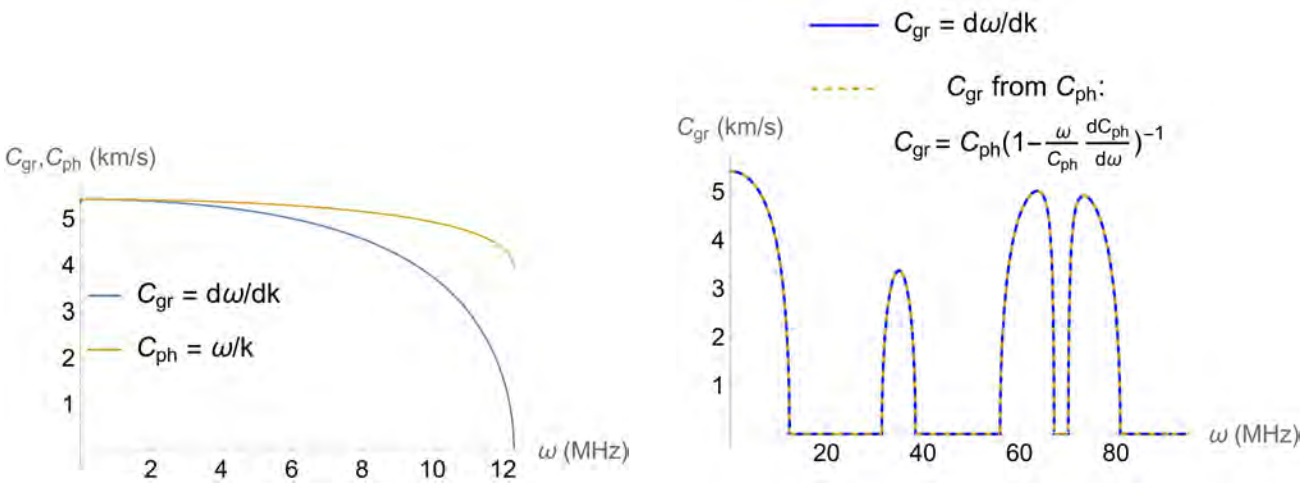

(a) (b)

Fig. 12 (a) Group C_{gr} and phase C_{ph} velocities vs. frequency derived from the first pass band in Fig. 11(a), and (b) group velocities vs. frequency for the first four pass bands in Fig. 11(a) determined using the frequency spectrum plotted using the extended zone scheme, cf., Fig. 2. of Lee and Yang[29]

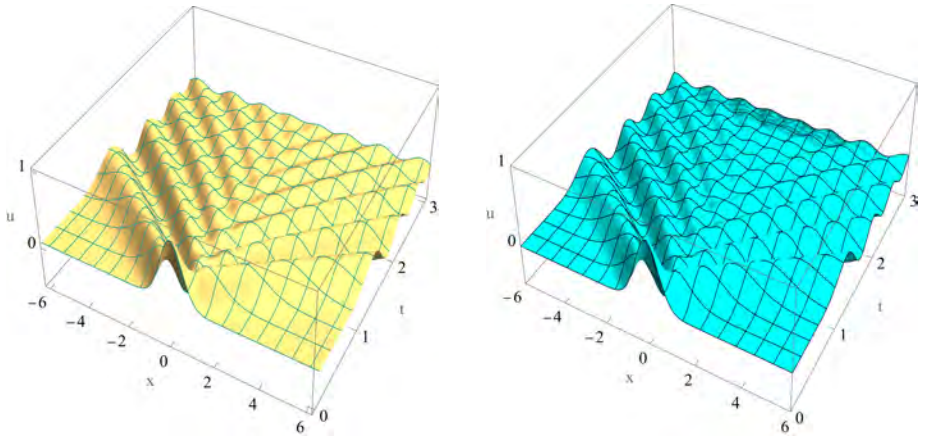

(a) (b)

Fig. 13 Numerical solutions to the nonlocal IVP given by a Gaussian initial displacement field cf., Eq. 39_1 and dispersion relation $\omega(k) = \sqrt{a\left(1 - e^{-\frac{1}{2}b^2k^2}\right)}$ using (a) IFFT evaluation of Eq. 54 (AT = 11 s), (b) series solution given by Eq. 55 (AT = 286 s)

8. Conclusions

An IFFT algorithm was developed to solve IVPs for wave propagation in nonlocal peridynamic media. For IVPs involving continuous initial conditions, the IFFT solutions compared well with solutions obtained using Mathematica's NIntegrate function[7] and verified using the Bessel series solutions developed by Beyer et al.[1] The NIntegrate function and IFFT algorithm solutions were all generally computed in less than 1 min of CPU time; one solution, however, using Mathematica's NIntegrate function with the "GaussKronrodRule" required 3.63 h of CPU time on 48 processors cf., Table 1. The accuracy of Mathematica's NIntegrate function and the IFFT algorithm was diminished cf., Table 1, however, for IVPs involving discontinuous initial conditions, particularly in the vicinity of the jump discontinuity where Mathematica's plotting functions "ListPlot3D" and "Plot3D" plotted a continuous surface for the solution jumps in Figs. 7 through 10. The Mathematica NIntegrate and IFFT solution algorithms are provided in Appendixes A and B, respectively, so that users can evaluate them in order to improve the speed and accuracy of IVPs involving discontinuous initial conditions. Solution accuracy might be improved in IVPs with discontinuous inital conditions, using Fourier reconstruction methods for piecewise-smooth functions.[33]

A nonlinear dispersion relation using Floquet theory was derived for a periodic elastic medium of infinite extent, which was used to solve an IVP that compared well with the series solution method of Beyer et al.[1] where it was first necessary to determine the $k^{th}-$convolution of the micromodulus function with the initial condition. The Mathematica IFFT and Bessel series solution algorithms are provided in the Appendixes C and D, respectively.

A local-nonlocal peridynamic correspondence principle was identified, which enabled direct determination of nonlocal Fourier transform domain solutions to IVPs from the local Fourier transform domain solutions; the correspondence principle only requires identification of the nonlinear dispersion curve for the material and does not require definition of a micromodulus function, although the latter is implicitly defined via an integral equation. Results are useful for modeling and verification of dispersive wave propagation in large-scale peridynamic numerical simulations.

Finally, Appendix E includes some notes relevant to problems where the Fourier transform is applied to the balance of linear momentum for a local continuum, and

where we assume that the displacements $u = u(x,t)$ are continuous functions of position and time, so that jump in u is identically zero, i.e., $[\![u]\!] = 0$, but that $[\![\sigma]\!] \neq 0$ and $[\![v]\!] \neq 0$. In Appendix F, we study the consequence of allowing for a jump discontinuity in u, i.e., in assuming that $[\![u]\!] \neq 0$, in solutions to IVPs with discontinuous initial conditions (cf., Problem 3 and Eq. 42) that involve the 1-D local wave equation; future work may consider application to the nonlocal equation of linear momentum given by Eq. 1.

9. References

1. Beyer HR, Aksoylu B, Celiker F. On a class of nonlocal wave equations from applications. Journal of Mathematical Physics. 2016;57:062902.

2. Aksoylu B, Gazonas GA. On the choice of kernel function in nonlocal wave propagation. Journal of Peridynamics and Nonlocal Modeling. 2020;2:379–400.

3. Kunin I. Elastic media with microstructure I: One-dimensional models. Springer-Verlag; 1982.

4. Silling SA, Zimmerman M, Abeyaratne R. Deformation of a peridynamic bar. Journal of Elasticity. 2003;73:173—190.

5. Weckner O, Abeyaratne R. The effect of long-range forces on the dynamics of a bar. Journal of the Mechanics and Physics of Solids. 2005;53:705—728.

6. Gazonas GA, Aksoylu B, Wildman RA. Fast solution of initial value problems for wave propagation in nonlocal media. Paper presented at: USACM Thematic Conference on Nonlocal Methods in Fracture. 2018 Jan 15–16; University of Texas, Austin, Texas.

7. Wolfram Research, Mathematica edition: version 12.3.0.0. 2021.

8. Lanczos C. Linear differential operators. Van Nostrand; 1961.

9. Gazonas GA, Wildman RA, Hopkins DA, Scheidler MJ. Longitudinal impact into viscoelastic media. Archive of Applied Mechanics. 2018;88(8):1275–1304.

10. Emmrich E, Weckner O. Analysis and numerical approximation of an integro-differential equation modeling non-local effects in linear elasticity. Mathematics and Mechanics of Solids. 2007;12:363–384.

11. Jafarzadeh S, Wang L, Larios A, Bobaru F. A fast convolution-based method for peridynamic transient diffusion in arbitrary domains. Computer Methods in Applied Mechanics and Engineering. 2021;375:113633.

12. Jafarzadeh S, Mousavi F, Larios A, Bobaru F. A general and fast convolution-based method for peridynamics: Applications to elasticity and brittle fracture. Computer Methods in Applied Mechanics and Engineering. 2022;375:114666.

13. Coclite GM, Fanizzi A, Lopez L, Maddalena F, Pellegrino SF. Numerical methods for the nonlocal wave equation of the peridynamics. Applied Numerical Mathematics. 2020;155:119–139.

14. Eringen AC. Linear theory of nonlocal elasticity and dispersion of plane waves. International Journal of Engineering Science. 1972;10:425—435.

15. Velo AP, Gazonas GA, Bruder E, Rodriguez N. Recursive dispersion relations in one-dimensional periodic elastic media. SIAM Journal of Applied Mathematics. 2008;69(3):670—689.

16. Weckner O, Silling SA. Determination of nonlocal constitutive equations from phonon dispersion curves. Journal for Multiscale Computational Engineering. 2011;9(6):623–634.

17. Silling SA. Propagation of a stress pulse in a heterogeneous elastic bar. Journal of Peridynamics and Nonlocal Modeling. 2021;3:255—275.

18. Weinberger HF. A first course in partial differential equations. John Wiley & Sons; 1965.

19. Walton J. Mathematics 603 Class Notes. Texas A&M University Lecture; 1983.

20. Silling S, Epton M, Weckner O, Xu J, Askari E. Peridynamic states and constitutive modeling. Journal of Elasticity. 2007;88:151–184.

21. Carcione JM, Kosloff D, Kosloff R. Wave propagation simulation in a linear viscoacoustic medium. Geophysical Journal. 1988;93:393—407.

22. Herrera I, Gurtin ME. A correspondence principle for viscoelastic wave propagation. Quarterly of Applied Mathematics. 1965;22(4):360—364.

23. Christensen RM. Theory of viscoelasticity: An introduction. Academic Press; 1982.

24. Bracewell RM. The Fourier transform and its applications. McGraw Hill; 1965.

25. Chen CT. One-dimensional digital signal processing. Marcel Dekker; 1979.

26. Gazonas GA, Scheidler MJ, Velo AP. Exact analytical solutions for elastodynamic impact. International Journal of Solids and Structures. 2015;75–76:172–187.

27. Hrusa WJ, Renardy M. On wave propagation in linear viscoelasticity. Quarterly of Applied Mathematics. 1985;XLIII(2):237–254.

28. Young J. Performing Fourier transforms in Mathematica. 2007 Aug 1 [accessed 2017 Oct 26]. https://www.asc.ohio-state.edu/schumacher.60/class/8820.uf/project_09/young.pdf.

29. Lee EH, Yang H. On waves in composite materials with periodic structure. SIAM Journal of Applied Mathematics. 1973;25(3):492—499.

30. Esquivel-Sirvent R, Cocoletzi GH. Band structure for the propagation of elastic waves in superlattices. Journal of the Acoustic Society of America. 1994;95(1):86—90.

31. Pilant WL. Elastic waves in the earth: Developments in solid earth geophysics 11. Elsevier; 1979.

32. Ben-Menahem A, Singh SJ. Seismic waves and sources. Springer-Verlag; 1981.

33. Platte RB, Gutierrez AJ, Gelb A. Fourier reconstruction of univariate piecewise-smooth functions from non-uniform spectral data with exponential convergence rates. Applied and Computational Harmonic Analysis. 2015;39(3):427–449.

34. Sneddon IN. The linear theory of thermoelasticity. Springer Verlag; 1974.

35. Chadwick P, Powdrill B. Application of the Laplace transform method to wave motions involving strong discontinuities. Proc. Camb. Philos. Soc. 2016;60:313–324.

36. Martin PA. The pulsating orb: solving the wave equation outside a ball. Proc. R. Soc. A. 2016;472:20160037.

37. Davison L. Fundamentals of shock wave propagation in solids. Springer Verlag; 2008.

Appendix A. NIntegrate Mathematica Code for Problems 1 Through 4

CloseKernels[]; LaunchKernels[48]; MP = $MachinePrecision;

F[x_?NumericQ, t_?NumericQ]:=

NIntegrate $\left[\frac{1}{2}\text{Exp}[-\text{Abs}[k]]\text{Cos}[kt]\text{Exp}[ikx], \{k, -\infty, \infty\}\right.$, AccuracyGoal → MP,

WorkingPrecision → MP, MaxRecursion → 60,

Method → {"DoubleExponential", "SymbolicProcessing" → 0}];

NIntProb1 = Chop[ParallelTable[$F[x, t]$, $\{t, 0, 5, 1/10\}$, $\{x, -5, 5, 1/10\}$]]; //

AbsoluteTiming

F[x_?NumericQ, t_?NumericQ]:=

NIntegrate $\left[\frac{1}{2\pi}\text{Cos}\left[t\sqrt{1-\text{Exp}\left[\frac{-k^2}{2}\right]}\right]\text{Exp}\left[-k^2/\,8\right]\text{Exp}[ikx], \{k, -\infty, \infty\}\right.$,

AccuracyGoal → MP, WorkingPrecision → MP, MaxRecursion → 60,

Method → {"DoubleExponential", "SymbolicProcessing" → 0}];

NIntProb2 = Chop[ParallelTable[$F[x, t]$, $\{t, 0, 20, 1/10\}$, $\{x, -6, 6, 1/10\}$]]; //

AbsoluteTiming

F[x_?NumericQ, t_?NumericQ]:=

NIntegrate $\left[\frac{1-ik}{2\pi(1+k^2)}\text{Cos}[kt]\text{Exp}[ikx], \{k, -300, 300\}\right.$,

AccuracyGoal → MP, WorkingPrecision → 6MP, MaxRecursion → 60,

Method → {"GaussKronrodRule", "SymbolicProcessing" → 0}];

NIntProb3 = Chop[ParallelTable[$F[x, t]$, $\{t, 0, 5, 1/10\}$, $\{x, -5, 5, 1/10\}$]]; //AbsoluteTiming

F[x_?NumericQ, t_?NumericQ]:=

NIntegrate $\left[\frac{1-ik}{2\pi(1+k^2)}\text{Cos}\left[t\sqrt{1-\text{Exp}\left[-k^2/\,2\right]}\right]\text{Exp}[ikx]\right.$,

$\{k, -300, 300\}$, AccuracyGoal → MP, WorkingPrecision → 6MP, MaxRecursion →

60, Method → {"GaussKronrodRule", "SymbolicProcessing" → 0}];

NIntProb4 = Chop[ParallelTable[$F[x, t]$, $\{t, 0, 20, 1/10\}$, $\{x, -6, 6, 1/10\}$]]; //AbsoluteTiming

Appendix B. IFFT Mathematica Code for Problems 1 Through 4

CloseKernels[]; LaunchKernels[48]; MP = $MachinePrecision;

$n = 2^{14}$; dk = $\frac{1}{10\sqrt{10}}$; Dv = $N[2\pi/(n\text{dk})]$;

F[k_?NumericQ, t_?NumericQ]:=πCos[dkkt]Exp[$-$Abs[dk$k$]];

ifft1 = Chop[ParallelTable[$g = N$[Table[$F[k,t]$, $\{k, -(n/2), n/2\}$], MP];

IFFTValues = InverseFourier[RotateLeft[$g, n/2{-}1$], FourierParameters $\to \{1, -1\}$];

IFFTValue = Chop[RotateRight[IFFTValues/Dv, $n/2{-}1$]], $\{t, 0, 20, 1/10\}$]]; //AbsoluteTiming

$n = 2^{14}$; dk = $\frac{1}{10\sqrt{10}}$; Dv = $N[2\pi/(n\text{dk})]$;

F[k_?NumericQ, t_?NumericQ]:=Cos $\left[t\sqrt{1 - \text{Exp}\left[\frac{-(\text{dk}k)^2}{2}\right]}\right]$ Exp $[-(\text{dk}k)^2/\,8]$;

ifft2 = Chop[ParallelTable[$g = N$[Table[$F[k,t]$, $\{k, -(n/2), n/2\}$], MP];

IFFTValues = InverseFourier[RotateLeft[$g, n/2{-}1$], FourierParameters $\to \{1, -1\}$];

IFFTValue = Chop[RotateRight[IFFTValues/Dv, $n/2{-}1$]], $\{t, 0, 20, 1/10\}$]]; //AbsoluteTiming

$n = 2^{14}$; dk = $\frac{1}{10\sqrt{10}}$; Dv = $N[2\pi/(n\text{dk})]$;

F[k_?NumericQ, t_?NumericQ]:=Sinc $\left[\frac{2\pi\, k}{n}\right]$ $\frac{1-i\text{dk}k}{(1+(\text{dk}k)^2)}$Cos[dk$kt$];

ifft3 = Chop[ParallelTable[$g = N$[Table[$F[k,t]$, $\{k, -(n/2), n/2\}$], MP];

IFFTValues = InverseFourier[RotateLeft[$g, n/2{-}1$], FourierParameters $\to \{1, -1\}$];

IFFTValue = Chop[RotateRight[IFFTValues/Dv, $n/2{-}1$]], $\{t, 0, 20, 1/10\}$]]; //AbsoluteTiming

$n = 2^{14}$; dk = $\frac{1}{10\sqrt{10}}$; Dv = $N[2\pi/(n\text{dk})]$;

F[k_?NumericQ, t_?NumericQ]:=Sinc $\left[\frac{2k\pi}{n}\right]$ $\frac{1-i\text{dk}k}{(1+(\text{dk}k)^2)}$Cos $\left[t\sqrt{1 - \text{Exp}\left[-(\text{dk}k)^2/\,2\right]}\right]$;

ifft4 = Chop[ParallelTable[$g = N$[Table[$F[k,t]$, $\{k, -(n/2), n/2\}$], MP];

IFFTValues = InverseFourier[RotateLeft[$g, n/2{-}1$], FourierParameters $\to \{1, -1\}$];

IFFTValue = Chop[RotateRight[IFFTValues/Dv, $n/2{-}1$]], $\{t, 0, 20, 1/10\}$]]; //AbsoluteTiming

Appendix C. Mathematica Notebook for the IFFT Solution of Eq. 54 and Shown in Fig. 13(a)

$n = 2^{14}$; dk $= 1/(10\sqrt{10})$; Dv $= N[2\pi/(n\,\text{dk})]$; $a = 205.680$; $b = 0.557383$;

space $=$ Table[Dv$(i - n/2), \{i, 1, n\}]$; ifft $=$ Chop[ParallelTable[

$$g = N\left[\text{Table}\left[\text{Cos}\left[t\sqrt{a\left(1 - e^{-\frac{b^2\text{dk}^2k^2}{2}}\right)}\right]e^{-\frac{\text{dk}^2k^2}{8}}, \{k, -(n/2), n/2\}\right]\right];$$

IFFTValues $=$ InverseFourier[RotateLeft$[g, n/2-1]$, FourierParameters $\rightarrow \{1, -1\}$];

IFFTValue $=$ Chop[RotateRight[IFFTValues/Dv$, n/2 - 1]], \{t, 0, 3, 1/20\}]]$;

IFFTsirventcocoletzsoln $=$

ListPlot3D[Re[ifft], DataRange $\rightarrow \{\{$space$[[1]]$, space$[[n]]\}, \{0, 3\}\}$,

PlotRange $\rightarrow \{\{-6, 6\}, \{0, 3\}, \{-.5, 1\}\}$, Mesh $\rightarrow 20$, AspectRatio $\rightarrow 1$,

Ticks $\rightarrow \{\{-6, -4, -2, 0, 2, 4, 6\}, \{0, 1, 2, 3\}, \{0, 1\}\}$,

BaseStyle $\rightarrow \{$FontFamily $\rightarrow$ "Times", FontSize $\rightarrow 14\}$,

AxesEdge $\rightarrow \{\{-1, -1\}, \{1, -1\}, \{-1, -1\}\}$, AxesLabel $\rightarrow \{$x, t, u$\}$,

ViewPoint $\rightarrow \{1.3, -2.4, 2\}]$

Appendix D. Mathematica Notebook for the Series Solution Given by Eq. 55 and Shown in Fig. 13(b)

a = 205.680; b = 0.557383;Beyersirventcocoletzsoln =

Plot3D[$\Big($$e^{-2x^2}\sqrt{\frac{2}{\pi}}$Cos $[\sqrt{a}t]$ +

$\sqrt{\frac{2}{\pi}}$ ParallelSum[$\frac{\left(\sqrt{a}t\right)^{k+1}}{2^k\,k!}$SphericalBesselJ $[k-1, \sqrt{a}t]$ $\frac{e^{-\frac{2x^2}{1+4\,k\,b^2}}}{\sqrt{1+4\,k\,b^2}}$, $\{k, 1, 75\}$]$\Big)$,

$\{x, -6, 6\}, \{t, 0, 3\},$ PlotRange $\rightarrow \{\{-6, 6\}, \{0, 3\}, \{-0.5, 1.0\}\},$

Ticks $\rightarrow \{\{-6, -4, -2, 0, 2, 4, 6\}, \{0, 1, 2, 3\}, \{0, 1\}\},$

BaseStyle $\rightarrow \{$FontFamily $\rightarrow$ "Times", FontSize $\rightarrow 14\}$, PlotPoints $\rightarrow 100,$

AspectRatio $\rightarrow 1,$ AxesEdge $\rightarrow \{\{-1, -1\}, \{1, -1\}, \{-1, -1\}\},$

AxesLabel $\rightarrow \{$x, t, u$\}$, MeshStyle $\rightarrow$ RGBColor$[0/255, 139/255, 139/255],$

ColorFunction $\rightarrow$ (RGBColor$[255/255, 210/255, 115/255]\&$),

ViewPoint $\rightarrow \{1.3, -2.4, 2\}]$

Appendix E. Fourier Transform of the Local Balance of Momentum Equation by Assuming $[\![u]\!] = 0$

The balance of linear momentum for a local continuum is given by

$$\rho\,\frac{\partial v}{\partial t}\;=\pm\,\frac{\partial \sigma}{\partial x}\,. \tag{E-1}$$

For a function $f(x)$ that is only piecewise continuous and piecewise smooth, the rule for the Fourier transform of its first derivative $\mathcal{F}\{f^1(x) : x \to k\} = (i\,k)\widehat{f}(k)$ (cf., Eq. 17) is not valid, and the correct relation is*

$$\mathcal{F}\big\{\,f^1(x)\,\big\}(k) = (i\,k)\,\widehat{f}(k) - \sum_{n\geq 1} [\![f]\!](x_n)\,e^{-i\,k\,x_n}\,, \tag{E-2}$$

where $x_1 < x_2 < \ldots$ is the (finite or infinite) sequence of positions at which f suffers a jump discontinuity, and $[\![f]\!](x_n) = f(x_n^+) - f(x_n^-)$.†

Let $x_1(t) < x_2(t) < \ldots$ denote the infinite sequence of positions at which the shock arrives at time t in say a finite target under impact. That is, $x_n(t)$ is the position at which the shock arrives at time t on its nth one-way trip across the target. Then on applying Eq. $\mathrm{E}-2$ to $f(x) = \sigma(x,t)$, we obtain

$$\mathcal{F}\big\{\frac{\partial \sigma(x,t)}{\partial x}\big\}(k,t) = (i\,k)\,\widehat{\sigma}(k,t) - \sum_{n=1}^{\infty} [\![\sigma]\!]\big(x_n(t),t\big)\,e^{-i\,k\,x_n(t)}\,. \tag{E-3}$$

This is the correct expression for the term $\mathcal{F}\big\{\frac{\partial \sigma(x,t)}{\partial x}\big\}$ that appears on the right side of the Eq. $\mathrm{E}-1$ for the Fourier transform of the momentum balance.

Now consider the term on the left-hand side of Eq. $\mathrm{E}-1$. We have

$$\mathcal{F}\big\{v\big\}(k,t) = \int_{-\infty}^{\infty} v(x,t)\,e^{-i\,k\,x}dx = \sum_{n=1}^{\infty}\int_{x_{n-1}(t)}^{x_n(t)} v(x,t)\,e^{-i\,k\,x}dx\,, \tag{E-4}$$

where $x_0(t) \equiv 0$. It is not hard to see that for $n \geq 1$,

$$x_n(t) = \begin{cases} c\,t - (n-1)\,l & \text{if } \; n = 1,3,5,\ldots; \\ \\ n\,l - c\,t & \text{if } \; n = 2,4,6,\ldots, \end{cases} \tag{E-5}$$

*cf., pg. 182, Eq. A.2 of Sneddon,[34] where the definition of the Fourier transform of $\widehat{f}(k) = \mathcal{F}\{f(x) : x \to k\} \equiv \frac{1}{\sqrt{2\pi}}\int\limits_{-\infty}^{\infty} f(x)\,e^{i\,k\,x}\,dx$ differs from that used in Eq. 13.

†In this Appendix E we assume that the displacements $u = u(x,t)$ are continuous functions of position and time so that jump in u is identically zero, $[\![u]\!] = 0$, but that $[\![\sigma]\!] \neq 0$ and $[\![v]\!] \neq 0$.

where c is the shock wave *speed*. By Eq. $\mathrm{E}-5$,

$$\frac{d}{dt}\, x_n(t) = c(-1)^{n-1}\,, \quad n = 1, 2, 3, \ldots\,, \tag{E-6}$$

independent of t. Next, we take the partial derivative of Eq. $\mathrm{E}-4$ with respect to t and use Leibniz's rule for the derivative of an integral with variable limits of integration. Then on using Eq. $\mathrm{E}-6$ in the result and rearranging terms, we obtain*

$$\frac{\partial}{\partial t}\,\mathcal{F}\{v\}(k,t) = \mathcal{F}\left\{\frac{\partial v}{\partial t}\right\}(k,t) + c\sum_{n=1}^{\infty}(-1)^n\,[\![v]\!]\big(x_n(t),t\big)\,e^{-i\,k\,x_n(t)}\,. \tag{E-7}$$

On substituting Eqs. $\mathrm{E}-7$ and $\mathrm{E}-3$ into Eq. $\mathrm{E}-1$ for the Fourier transform of balance of momentum, we obtain

$$i\,k\,\widehat{\sigma}(k,t) \,+\, \rho\frac{\partial}{\partial t}\,\widehat{v}(k,t) \;=\; \sum_{n=1}^{\infty}\Big((-1)^n\,\rho\,c\,[\![v]\!] + [\![\sigma]\!]\Big)\big(x_n(t),t\big)\,e^{-i\,k\,x_n(t)}\,. \tag{E-8}$$

We claim that the right-hand side of Eq. $\mathrm{E}-8$ is zero. Indeed, when stress is taken positive in compression the jumps in stress and particle velocity across a shock are related by†

$$[\![\sigma]\!] = \rho U [\![v]\!]\,, \tag{E-9}$$

where U is the intrinsic or referential *velocity* of the wave front,

$$U(t) = \frac{d}{dt}\,Y(t)\,, \tag{E-10}$$

and $Y(t)$ is the position of the shock front at time t. For a linear elastic material and finite thickness target, $|U(t)| = c$, independent of the time t, but during the nth one-way trip of the shock,

$$U(t) = (-1)^{n+1}c\,. \tag{E-11}$$

$U(t)$ is positive for odd n, when the wave is traveling in the positive x-direction (i.e., toward the back face); and $U(t)$ is negative for even n, when the wave is

*Observe that up to this point we have not made use of the fact that v is a velocity component; hence Eq. $\mathrm{E}-7$ holds for other piecewise continuous and piecewise smooth functions with jumps across the shock only. See also the interesting papers by Chadwick and Powdrill[35] and Martin[36] for the multi-dimensional Laplace transform analog of Eq. $\mathrm{E}-7$ for a single jump; i.e., they do not treat the case of multiple reflections as treated by Gazonas et al.[9] Also, by $\mathrm{E}-7$ it follows that we may interchange the Fourier transform and the partial derivative with respect to t for continuous and piecewise smooth functions.

†cf., Davison.[37]

traveling in the negative x-direction (i.e., toward the front face). From Eqs. $\mathrm{E}-9$ and $\mathrm{E}-11$, we see that

$$[\![\sigma]\!]\big(x_n(t),t\big) = \rho(-1)^{n+1}c[\![v]\!]\big(x_n(t),t\big)\,. \tag{E-12}$$

When this is substituted into Eq. $\mathrm{E}-8$, the terms inside the large parentheses cancel so that the right-hand side is zero, which yields the correct Fourier transform of Eq. $\mathrm{E}-1$.

Appendix F. Fourier Transform of the Local Wave Equation by Assuming $[\![u]\!] \neq 0$

In this Appendix F we study the consequence of allowing for a jump discontinuity in u i.e., in assuming that $[\![u]\!] \neq 0$ in solutions to IVPs with discontinuous initial conditions (cf., Problem 3 and Eq. 42) that involve the 1-D the wave equation:

$$\frac{\partial^2 u}{\partial t^2} = c^2 \frac{\partial^2 u}{\partial x^2} \,. \tag{F-1}$$

On taking the time-derivative of the Fourier transform (Eq. 13) of u where $[\![u]\!] \neq 0$ we arrive at,

$$\frac{\partial}{\partial t}\mathcal{F}\{u\} = \mathcal{F}\{\frac{\partial u}{\partial t}\} + [\![u]\!]\, e^{-i\,k\,x}\frac{\partial x}{\partial t} \,. \tag{F-2}$$

Further, on replacing u by $\frac{\partial u}{\partial t}$ in Eq. $\mathrm{F}-2$ and after rearrangement of terms obtain,

$$\mathcal{F}\{\frac{\partial^2 u}{\partial t^2}\} = \frac{\partial}{\partial t}\mathcal{F}\{\frac{\partial u}{\partial t}\} - [\![\frac{\partial u}{\partial t}]\!]\, e^{-i\,k\,x}\frac{\partial x}{\partial t} \,. \tag{F-3}$$

On solving for the first term on the right-hand side of Eq. $\mathrm{F}-2$ with $\mathcal{F}\{u\} = \widehat{u}$, and substituting this into the first term on the right-hand side of Eq. $\mathrm{F}-3$ results in,

$$\mathcal{F}\{\frac{\partial^2 u}{\partial t^2}\} = \frac{\partial}{\partial t}\Big(\frac{\partial \widehat{u}}{\partial t} - [\![u]\!]\, e^{-i\,k\,x}\frac{\partial x}{\partial t}\Big) - [\![\frac{\partial u}{\partial t}]\!]\, e^{-i\,k\,x}\frac{\partial x}{\partial t} \,, \tag{F-4}$$

or,

$$\mathcal{F}\{\frac{\partial^2 u}{\partial t^2}\} = \frac{\partial^2 \widehat{u}}{\partial t^2} - \Big(\frac{\partial [\![u]\!]}{\partial t}\,\frac{\partial x}{\partial t} + [\![u]\!]\,\frac{\partial^2 x}{\partial t^2} - i\,k\,[\![u]\!]\,(\frac{\partial x}{\partial t})^2 + [\![\frac{\partial u}{\partial t}]\!]\,\frac{\partial x}{\partial t}\Big)\, e^{-i\,k\,x} \,, \tag{F-5}$$

which parallels the Laplace transform development of Martin[36] (cf., Eq. 8.2 on pg. 16) i.e., $\mathcal{L}\{\nabla^2 u\}$. For the spatial derivatives appearing on the right-hand side of Eq. $\mathrm{F}-1$ we arrive at,

$$\mathcal{F}\{\frac{\partial^2 u}{\partial x^2}\} = -k^2\,\widehat{u} + \Big(i\,k\,[\![u]\!] + [\![\frac{\partial u}{\partial x}]\!]\Big)\, e^{-i\,k\,x} \,. \tag{F-6}$$

1 (PDF) DEFENSE TECHNICAL INFORMATION CTR DTIC OCA

1 (PDF) DEVCOM ARL FCDD RLD DCI TECH LIB

1 (PDF) CARNEGIE MELLON UNIVERSITY K DAYAL

3 (PDF) MASSACUSETTS INST TECH R RADOVITZKY R ABEYARATNE K KAMRIN

1 (PDF) UNIV SAN DIEGO AP VELO

2 (PDF) UNIV NEBRASKA F BOBARU P RADU

1 (PDF) UNIV ARIZONA E MADENCI

2 (PDF) LOUSIANA STATE UNIV R LIPTON P DIEHL

4 (PDF) SANDIA NATL LABS S SILLING D LITTLEWOOD ML PARKS R WILDMAN

1 (PDF) OAK RIDGE NATL LAB P SELESON

2 (PDF) UNIV STRATHCLYDE E OTERKUS S OTERKUS

3 (PDF) UNIV PADOVA U GALVANETTO F SCABBIA M ZACCARIOTTO

2 (PDF) UNIV TEXAS J FOSTER C LANDIS

1 (PDF) TEXAS TECH UNIV A IDESMAN

1 (PDF) TEXAS A&M UNIV-SA B AKSOYLU

1 (PDF) INST TEC SUP URUAPAN HR BEYER

1 (PDF) WAYNE STATE UNIV F CELIKER

1 (PDF) BOEING O WECKNER

ABERDEEN PROVING GROUND

25 (PDF) DEVCOM ARL
FCDD RLD
P BAKER
FCDD RLW
J ZABINSKI
FCDD RLW M
E CHIN
FCDD RLW MA
T BOGETTI
CF YEN
FCDD RLW MB
B LOVE
A GAYNOR
E HERNANDEZ
B POWERS
Z WILSON
G GAZONAS
FCDD RLW MC
C RINDERSPACHER
FCDD RLW TA
S BILYK
M GREENFIELD
FCDD RLW TB
S SATAPATHY
FCDD RLW TC
J CAZAMIAS
J CLAYTON
J LLOYD
B LEAVY
M FERMEN-COKER
FCDD RLW TD
C RANDOW
R DONEY
FCDD RLW TF
J OGRADY
FCDD RLW B
R BECKER
A TONGE